Ore Geology Reviews 104 (2019) 403–421

Contents lists available at ScienceDirect

Ore Geology Reviews

journal homepage: www.elsevier.com/locate/oregeorev

Late Cretaceous paleoclimate change and its impact on uranium mineralization in the Kailu Depression, southwest Songliao Basin

Zenglian Xu[a,b,*], Jianguo Li[a,b], Qiang Zhu[a,b], Jialin Wei[a,b], Hongliang Li[c], Bo Zhang[a,b]

[a] Tianjin Centre, China Geological Survey, 300170 Tianjin, China
[b] Laboratory of Non-Fossil Energy Minerals, Tianjin Center of China Geological Survey, 300170 Tianjin, China
[c] Development Company of New Energy Sources of Liaohe Petroleum Exploration Bureau, CNPC, 124010 Panjin, China

ARTICLE INFO

Keywords:
Uranium mineralization
Paleoclimate
Palynology
Late Turonian to early Campanian
Kailu Depression

ABSTRACT

Paleoclimate significantly influenced continental sandstone-type uranium mineralization. To better understand continental climate change in the Late Cretaceous and its influence on uranium mineralization, we selected four boreholes from Late Cretaceous sedimentary successions from the southwestern Songliao Basin, in northeastern China. Twenty-one samples were collected for sporopollen analyses. Based on the variations in the relative abundances of the different sporopollen taxa, we observed the four following palynological assemblages (PAs) in ascending order: the *Schizaeoisporites–Classopollis–Tricolporollenites* assemblage, the *Taxodiaceaepollenites–Exesipollenties–Cranwellia* assemblage, the *Schizaeoisporites–Classopollis–Lytharites* assemblage, and the *Biasccate–Taxodiaceaepollenites–Aquilapollenites* assemblage. Based on the geological range of several important elements and correlations between relevant assemblages from other regions, we assigned a geological age of late Turonian to early Campanian (approximately 86.7–84.4 Ma) to the four PAs. In this study, we introduced a sporopollen–climate transforming methodology, which uses the percentage of drought, hygrophilous, and thermophilic taxa to indicate stratigraphic trends of humidity and temperature. On the one hand, the percentage of thermophilic taxa was characterized by a continuously decreasing trend, but remained at a relatively high abundance along the entire sedimentary sequence. This was indicative of a hot subtropical–tropical climate with declining temperatures. On the other hand, the percentage of drought and hygrophilous taxa exhibited a cyclical fluctuation between humid and semi-arid climates. A semi-arid climate existed in the PA I, but this then changed to humid conditions in the PA II. Subsequently, the climate evolved into semi-arid and semi-humid conditions as a result of strengthened drought during the PA III. Finally, in the PA IV, the climate became humid once again. In general, the Yaojia Formation's synsedimentary paleoclimate (i.e., the PA II and PA III) mainly had semi-humid conditions. In the Qianjiadian area, the main prospect target layer is the Yaojia Formation. Compared with the typical sandstone-type uranium deposits throughout northern China, we suggest that the humid paleoclimate was essential for uranium mineralization. The humid climate favored the formation of reduced sandstones, which provided significant geochemical reducing barriers and uranium pre-concentrations essential for epigenetic uranium mineralization.

1. Introduction

As one of the largest Mesozoic and Cenozoic continental basins in northeastern China, the Songliao Basin contains a complete and well-preserved Mesozoic–Cenozoic strata (Chen and Chang, 1994; Wang et al., 2013a), with a maximum sedimentary thickness of approximately 10 km. Moreover, the Cretaceous strata comprise hydrocarbon zones and important uranium deposits. After more than 50 years of exploration and development, interesting results have been achieved with respect to both the basic geology and petroleum geology of the Songliao Basin (Chen and Chang, 1994; Deng et al., 2013; Feng et al., 2010a). The Cretaceous period is the most important greenhouse-effect period in the Earth's history (Friedrich et al., 2012; Huber et al., 2002; Hu, 2004; Skelton et al., 2003). The biological evolution, tectonic events, and mineralization during this period have an important effect on the present-day Earth system. Sporopollen data show large differentiations in the Cretaceous terrain of the Songliao Basin. The edge of the basin features mountains, whereas a relatively flat hillside or lake beach lay

Abbreviations: PA, palynological assemblage

* Corresponding author at: Tianjin Centre, China Geological Survey, 300170 Tianjin, China.
E-mail address: lz_xu870601@126.com (Z. Xu).

https://doi.org/10.1016/j.oregeorev.2018.10.020
Received 3 May 2018; Received in revised form 17 October 2018; Accepted 29 October 2018
Available online 30 October 2018
0169-1368/

between the mountain and the lake basin. In the mountains, vegetation consists mainly of coniferous forests, evergreen broad-leaved forests, and small amounts of deciduous broad-leaved forests. Plants, such as herbs and shrubs, grow on both the hillside and lakeside beaches. Coniferous forests, grasslands, and grasses, which represent a humid and semi-humid subtropical environment, dominate the overall vegetational landscape. Four cooling events, three warming events, and three drought events occurred during Cretaceous period (Wang et al., 2013a). Oxygen isotopic analyses on ostracoda fossils from the Qingshankou to Mingshui Formations within the Songliao Basin indicate that the Late Cretaceous experienced frequent changes in temperature, but was mostly characterized by a warm environment (Chamberlain et al., 2013). Climate change not only controls the rainfall, vegetation development, sediment types, and hydrological conditions, it also exerts an influence on hydrocarbon and uranium mineralization (Jiao et al., 2015; Li et al., 2004; Wu, 2005; Yang and He, 2016; Yu et al., 2005). The formation of oil and gas is closely related to vegetation development. The sediment type, paleohydrology, and oxidation–reduction conditions are also crucial to sandstone-type uranium deposit formation. Changes in the paleoclimate are traceable via important information that is recorded in the terrestrial strata. Studying changes in the paleoclimate is important when trying to understand the influence that paleoclimate has on sandstone-type uranium mineralization (Chen et al., 2011). This study can provide insights into the paleoclimate of the Qingshankou-Nenjiang Formation and its impact on uranium mineralization.

Several previous studies have shown that the climate in the Songliao Basin exhibits regional variations, but when discussing the paleoclimate, these studies have focused primarily on the central depression area (Ji et al., 2015; Li et al., 2011; Yoshino et al., 2017; Zhao et al., 2014). However, related paleoclimate studies in other areas of the Songliao Basin (especially the Kailu Depression) are rather scarce and prove inadequate when attempting to further geological knowledge in this region. On the other hand, braided fluvial and deltaic facies dominate the Qingshankou and Yaojia Formations in the Kailu Depression. These facies are characterized by sediments with coarse grain sizes, which is not favorable for microfossil preservation, such as sporopollen. Therefore, sporopollen fossils in this area are scarce and poorly preserved. As a result, the relationship between paleoclimate and uranium mineralization has received very little attention. In this study, to respond to the issues discussed above, we perform detailed descriptions and systematic sampling of fossils as well as their processing, analysis, and identification on a series of uranium exploration wells in the Qianjiadian area within the Kailu Depression. We divide and compare PAs, and then discuss their stratigraphic age. We also discuss the paleoclimatic changes in the Qingshankou-Nenjiang Formations and its geological significance with respect to the sandstone-type uranium mineralization using quantitative methods performed on the PAs.

2. Geological and Stratigraphic setting

2.1. Songliao Basin

Located in the northeastern part of China, the Songliao Basin is a large continental sedimentary basin that formed in the Late Mesozoic. The Songliao Basin is also the largest continental petroliferous basin in the world (Hou et al., 2009; Wang et al., 1994, 2013a). The Songliao Basin lies adjacent to the Hailar and Erlian Basin to the west and the Ordos Basin to the southwest (Fig. 1A). A series of mountains surround the Songliao Basin, i.e., the Zhangguangcailing Range to the southeast, the Lesser Xing'an Range to the northeast, and the Great Xing'an Range to the west (Deng et al., 2013). The basin is 750 km in length and 330–370 km in width, and it covers a total area of approximately 260,000 km^2 (Cheng, 1982; Daqing Oilfield Petroleum Geography Compilation Group, 1993; Liu et al., 1992; Song et al., 2014; Wang et al., 1994; Yang et al., 1982). Based on the Songliao Basin's Mesozoic structural evolution, basement morphology, and depositional characteristics, the basin can be divided into six first-order tectonic units: the western slope, the northern plunge, the central depression, the northeast uplift, the southeast uplift, and the southwest uplift (Fig. 1B) (Li et al., 2009; Zhu et al., 2014).

The Songliao Basin basement is comprised of Paleozoic metamorphic, igneous, and volcanic rocks (Feng et al., 2010a,b; Wang et al., 2013a,b). The sedimentary cover mainly consists of clastic deposits as old as the Late Jurassic, with a maximum thickness of approximately 10,000 m. The Songliao Basin was formed and filled in four tectonic stages (Fig. 2): mantle upwelling, rifting, post-rift thermal subsidence, and structural inversion (Feng et al., 2010a). During these four stages, three main tectonostratigraphic sequences formed (Wang et al., 2002; Wang and Chen, 2015): (i) The pre- and syn-rift tectonostratigraphic sequences (150–110 Ma), such as the Huoshiling (J_3h), Shahezi (K_1sh), and Yingcheng Formations (K_1y), which are characterized by the deposition of Late Jurassic volcanic rocks, alluvial, and lacustrine sediments that were deposited in isolated rift grabens, with a thickness of 3000 m; (ii) The post-rift tectonostratigraphic sequence (110–79.1 Ma), characterized by fluvial, deltaic, and lacustrine sediments with thicknesses of up to 4300 m. The post-rift sequence includes the Denglouku (K_1d), Quantou (K_1q), Qingshankou (K_1qn), Yaojia (K_1y), and Nenjiang Formations (K_1n). Continuous basin expansion is a typical feature during this interval. Two large-scale lake intrusions occurred in Member 1 of the Qingshankou Formation and Members 1 and 2 of the Nenjiang Formation. Characterized by a wide distribution, abundant organic matter, and a significant thickness, two sets of black shales, intercalated by oil shales, are the most important source and regional cap rocks in the Songliao Basin; (iii) The tectonic inversion tectonostratigraphic sequence (79.1–40 Ma) includes the Sifangtai (K_2s), Mingshui (K_2m), and Yi'an Formations (Ey). The tectonic inversion sequence is characterized by coarse clastic sediments from alluvial, fluvial, delta, and lacustrine facies, with an approximate thickness of 900 m.

2.2. Kailu Depression

The Kailu Depression, a Meso–Cenozoic fault-depression basin, is located in the southwestern part of the Songliao Basin (Fig. 1B) and has a total area of approximately 3.1×10^4 km^2. The depression lies in the Hercynian geosyncline fold basement. This basement is composed of pre-Sinian granite-gneiss and Carboniferous–Permian metamorphic rocks. The depression is filled with Cretaceous to Cenozoic clastic deposits (Fig. 1C). In the Early Cretaceous, the depression was an independent faulted basin. The volcanic rock and clastic sediments of lacustrine facies were then deposited, i.e., the Yixian, Jiufotang, Shahai, and Fuxin Formations. Afterward, during the Late Cretaceous, connections between the Kailu Depression, the Songliao Basin, and other depressions formed a large and unified basin. Upper Cretaceous variegated clastic rocks (i.e., the Quantou, Qingshankou, Yaojia, Nenjiang, Sifangtai, and Mingshui Formations) and Tertiary gray clastic rocks (i.e., the Yi'an, Da'an, and Taikang Formations) were then deposited (Chen et al., 2005). Here, the study area is located at the northeast limit of the Kailu Depression. Fig. 3A shows the specific distribution of the boreholes analyzed in this study. The studied section intersects the Qingshankou Formation's Member 3 and continues to the Nenjiang Formation's Member 1 (Fig. 3B).

The Qingshankou Formation (K_2qn), with a thickness of 0–236 m, is commonly observed in cores of regional anticlines. In this region, uplift

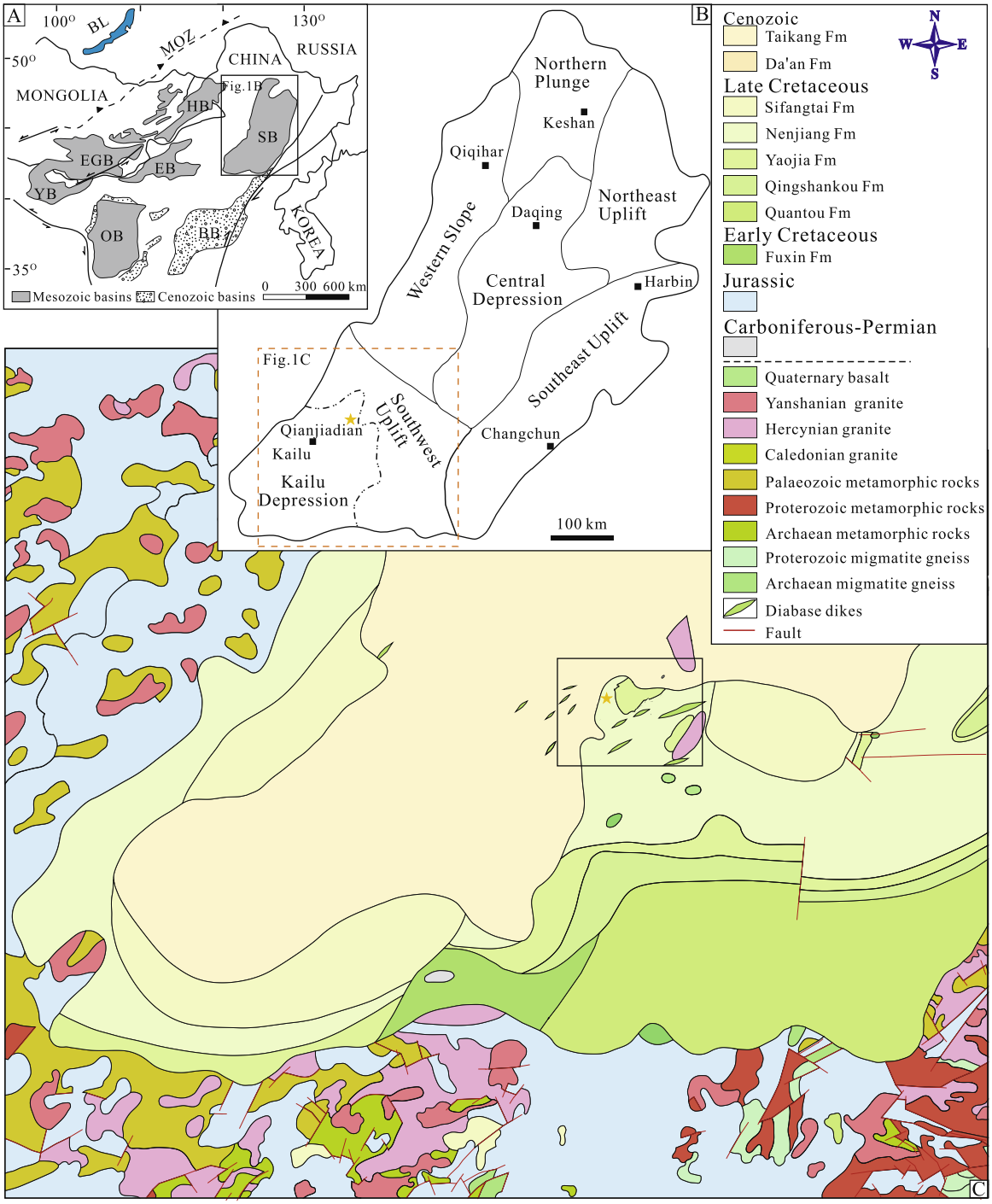

Fig. 1. A geological map of the Songliao Basin and study area. A) Structural map of Northeast China (modified after Bonnetti et al., 2014; Meng, 2003); BB = Bohai Basin, EB = Erlian Basin, EGB = East Gobi Basin, HB = Hailar Basin, OB = Ordos Basin, SB = Songliao Basin, YB = Yingen Basin, BL = Baikal Lake, MOZ = Mongol–Okhotsk Zone). B) Structural subdivisions of Songliao Basin (modified after Li et al., 2009; Scott et al., 2012; Zhao et al., 2013; Zhu et al., 2014); C) Geological map of the Kailu Depression.

and denudation are abundant, a condition which forms the common "skylight" structures. This formation occurs in NE–SW strips and has an angular unconformity with the underlying Fuxin Formation. The Qingshankou Formation's distribution widens towards the Shuangliao region. Gray mudstones and silty mudstones dominate the middle and lower parts of the Qingshankou Formation. The upper part is comprised of light gray glutenite, sandstone, and grayish green mudstone with positive rhythm, horizontal bedding, and wavy bedding.

The Yaojia Formation (K_2y), with a thickness of 60–240 m, was deposited in a fluvial environment. The Yaojia Formation shares an unconformity with the underlying Qingshankou Formation and spreads NE–SW as narrow strips, with increasing widths to the east of Tongliao.

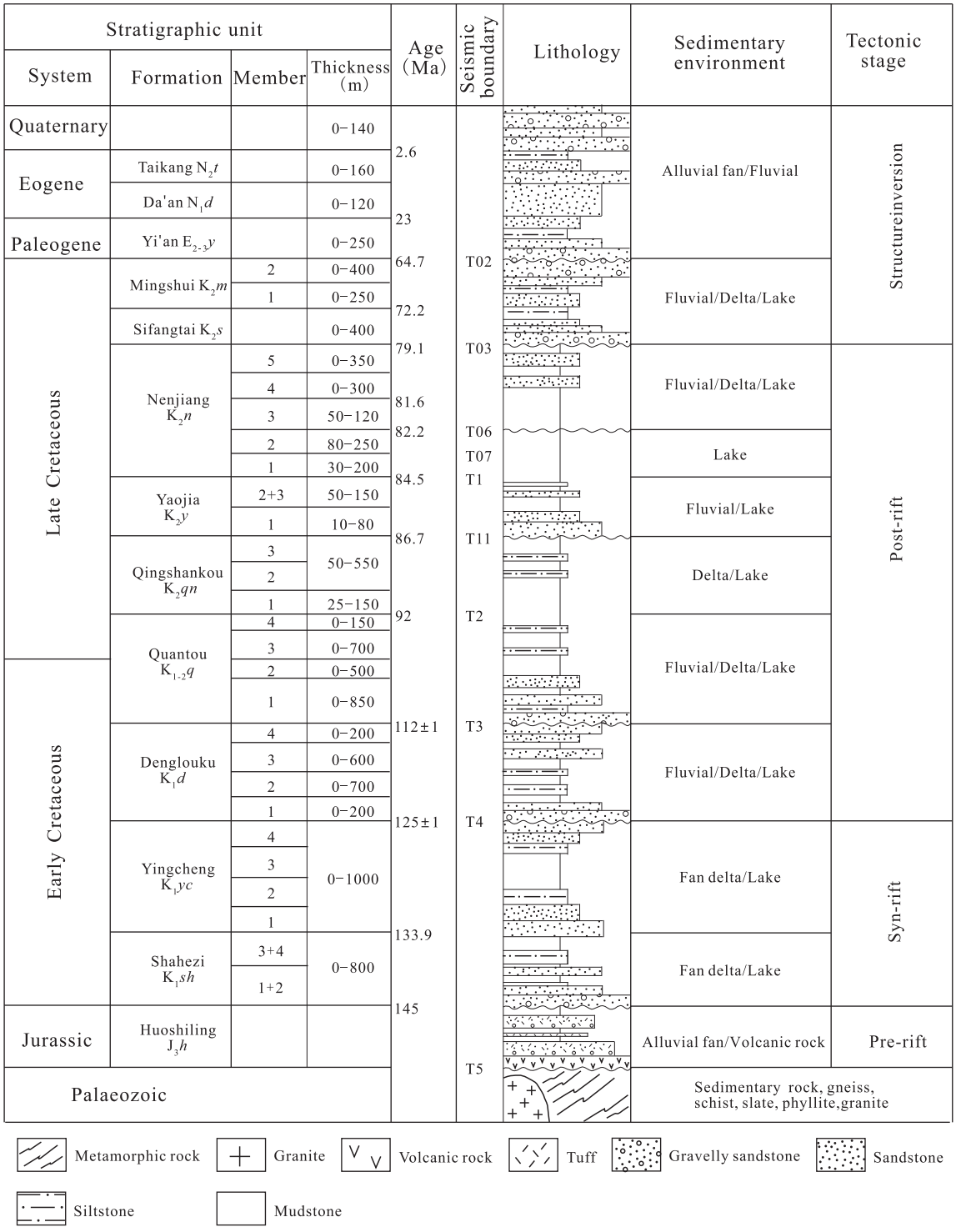

Fig. 2. Late Jurassic to Cenozoic tectono-stratigraphic evolution in the Songliao Basin (modified after Bonnetti et al., 2015; Feng et al., 2010a; Wang et al., 2002).

The lower part of the Yaojia Formation contains brownish red feldspathic coarse sandstone and small amounts of interlayered brownish red mudstone. The middle part of the Yaojia Formation is comprised of brownish red glutenite and mudstone. The upper part has gray, purple–red, and brownish red fine sandstone, interbedded with red mudstone. Based on a comprehensive analysis of core observations, logging data, and previous results (Xia, 2015), the Yaojia Formation can be divided into six sand groups: bottom-up Members Y1, Y2, Y3, Y4, Y5, and Y6, which we then compare with the boreholes (Fig. 3B).

The Nenjiang Formation (K_2n) overlies the Yaojia Formation and can be divided into three lithologic units. The lower part is composed of grayish green or gray–black mudstone interbedded with muddy siltstone, which contains a small number of pyrite grains. The middle part has gray–black mudstones, with horizontal bedding. The lower black mudstone is useful as a marker bed for stratigraphic correlation. The upper part contains gray and gray–black mudstone with a silty strip

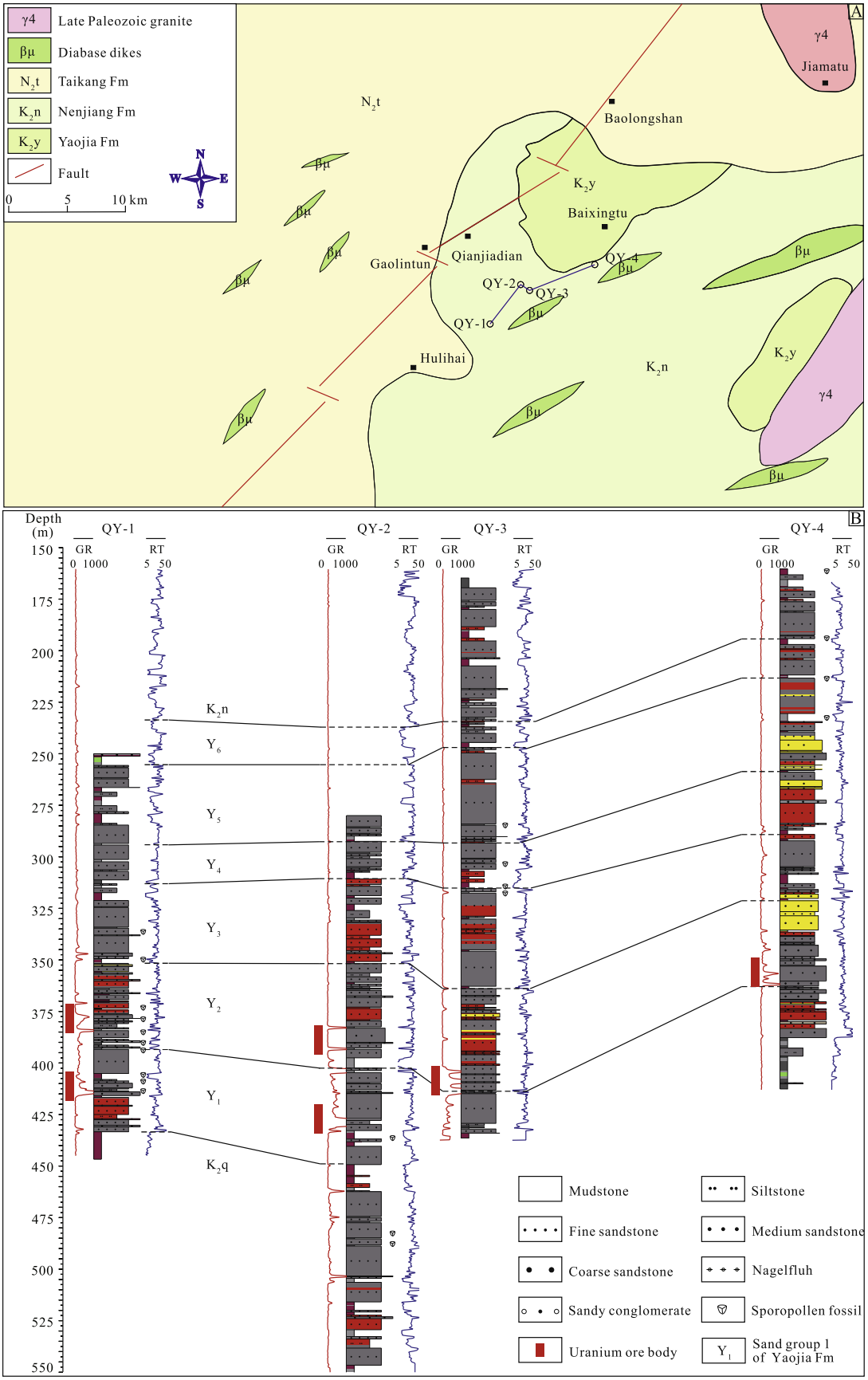

Fig. 3. A) The geological map of the study area with the location of the drill holes and the cross-section positions shown in B. B) Stratigraphic correlation in the drill holes and the distribution and location of the spore and pollen samples.

interlayer.

3. Materials and methods

Sporopollen fossil materials were collected from four wells (QY-1, QY-2, QY-3, and QY-4) throughout the Qianjiadian area of the Kailu Depression, in the southwestern part of the Songliao Basin (Fig. 3A). The average sampling distance was approximately 15 m. Based on the importance of the strata, lithological changes, and fossil contents, we further decreased (5 m) or increased (50 m) the sampling distance for some horizons. In this study, we collected 38 sporopollen samples, with a mudstone or silty mudstone lithology: 10 in QY-1, 7 in QY-2, 7 in QY-3, and 14 in QY-4. Based on comprehensive stratigraphic correlations, 21 samples were selected for sporopollen extraction and identification. Fig. 3B shows the specific location of each sample within the boreholes.

Sporopollen extraction and identification were performed at the Nanjing Institute of Geology and Palaeontology, Chinese Academy of Sciences. Sporopollen was treated with a hydrochloric acid–hydrofluoric acid mixture. The specific steps are as follows: (1) we obtained a total of 20–50 g of sample and ground it in a mortar to a particle size of less than 0.5 mm, (2) the ground sample was soaked in diluted hydrochloric acid (10%) and stirred thoroughly to remove the calcium, (3) fresh water was added, and the mixture stood for 3–4 h (we repeated this step until the mixture became neutral), (4) 250 mL of hydrofluoric acid was added slowly to the neutral mixture, then it was mixed thoroughly and allowed to stand for 5–7 days, (5) fresh water was then added and the mixture was allowed to stand (again, this step was repeated until the mixture became neutral), (6) the mixture was sieved (180 μm) to remove large particles, (7) approximately 300 mL of the sample was centrifuged to remove the water (3000 r/5 min), (8) concentrated hydrochloric acid (150 mL) was added, and the mixture was placed in an electric furnace for 2 h until the sample floated or the liquid clarified, (9) water was added to wash the sample (twice) until it became neutral, and (10) the sample was washed via a heavy liquid separation and sieving method. Fossil identification statistics and photography were both performed using a Zeiss Axio Scope A1 microscope.

In this study, we use the percentages of thermophilic, drought, and hygrophilous taxa in the PAs to visualize and understand climate change. The selection and calculation of thermophilic, drought, and hygrophilous taxa were mainly based on previous results (Abbink et al., 2001; Zhang et al., 2014; Gao et al., 1999).

4. Results

During statistical identification, we observed abundant, well-preserved sporopollen fossils (7963) in the 21 samples. On average, there were 379 fossils in each sample and up to 686 fossils in a single sample. In total, we identified 129 sporopollen fossils (Fig. 4), which were classified into 90 genera across 36 families. A small number of sporopollen types were not classified, but instead named according to their morphology (*Tricolpites* and *Retritricolporites*). Among the sporopollen, gymnosperm pollen (34 species in 26 genera, accounting for 21.1–86.3% of the assemblage, with an average of 55.3%) and pteridophyte spores (70 species in 46 genera, accounting for 13.4–75.5% of the assemblage, with an average of 42.8%) were the dominant types. We also identified angiosperm pollen (25 species in 18 genera, accounting for 0–5.0% of the assemblage, with an average of 1.9%). Figs. 5 and 6 show the major sporopollen species. Based on changes in the content and the appearance or disappearance of sporopollen groups, as well as other characteristics, we divided the sporopollenium species into four PAs in ascending order (Fig. 4). The various PAs characteristics are described below, from the base to the top.

4.1. Pollen results

PA I: *Schizaeoisporites–Classopollis–Tricolporollenites* (488.5–434.0 m). This palynomorph assemblage exhibits the following characteristics: Gymnosperm pollen is dominant (43.4–74.9%, with an average of 60.3%), pteridophyte spores have the second highest abundance (23.0–53.5%, with an average of 37.9%), and the angiosperm pollen content (0.3–3.1%, with an average of 1.8%) is the lowest. For the pteridophyte spores, *Schizaeoisporites* (Schizaeceae) are the most abundant, with an average of 26.9%. The high *Cyathidites* (Cyatheaceae) abundance also occurs continuously throughout the assemblage, accounting for approximately 3.4% of the assemblage. Ringed trilete spores, including *Polycingulatisporites* sp., *Foraminisporis* sp., *Nevesisporites* sp., and *Yichangsporites* sp., are also common. The remaining types are mostly trilete microspores with various grain, thorn, and tumor patterns, such as *Granulatisporites* sp., *Cyclogranisporites* sp., and *Apiculatisporis* sp. The gymnosperm pollen is characterized by a high abundance of *Classopollis*, with an average of 21.1%. Taxodiaceae, especially *Taxodiaceaepollenites hiatus,* have a high content, accounting for approximately 17.4% of the assemblage. The bisaccate conifer pollen, including *Pinuspollenites* sp., *Podocarpidites* sp., and *Protoconiferus* sp., accounts for 6.1% of the assemblage. *Exesipollenties*, including *E. tumulus* and *E. triangulus,* also appear continuously, representing only 5.5% of the total assemblage. Other common taxa, such as *Chasmatosporites* sp., *Cycadopites* sp., and *Psophosphaera* sp., are present but have minor importance. Angiosperm pollen is relatively monotonous, including *Retitricolpites* sp., *Tricolpopollenites* sp., and *Tricolporopollenites*sp.

PA II: *Taxodiaceaepollenites–Exesipollenties–Cranwellia* (413.2–349.5 m). The characteristics of this assemblage are as follows: Gymnosperm pollen is more abundant than the pteridophyte spores in this assemblage. The former accounts for 28.3–86.3%, with an average of 58.2%, while the latter accounts for 13.4–59.3%, with an average of 40.3%. The angiosperm pollen abundance is the lowest at 0.3–4.3%, with an average of 1.5%. For the pteridophyte spores, *Schizaeoisporites* (Schizaeceae) are characterized by a significant decrease compared with the PA I, which have an average content of 12.6%. The ringed spores, composed of *Polycingulatisporites* sp., *Foraminisporis* sp., *Nevesisporites* sp., and *Yichangsporites* sp., are subordinate, which account for an average of 9.4%. The *Cyathidites* (Polygonaceae) content has an average of 4.6%. We also observed certain amounts of other spores, such as *Cicatricosisporites* sp., *Retusotriletes* sp., and *Laevigatosporites* sp. The gymnosperm pollen content is dominated by *Exesipollenties* (average of 16.0%) and *Taxodiaceaepollenites hiatus* (average of 14.6%). A remarkable feature is the sharp decrease in the *Classopollis* (Cheirolepidiaceae) content from 21.1% to 9.8% in this assemblage. Bisaccate conifer pollen, composed of *Pinuspollenites* sp., *Podocarpidites* sp., *Piceites* sp., *Piceapollenites* sp., and *Protoconiferus* sp., is also common (8.0%). *Cycadopites* (average of 3.4%), *Chasmatosporites* (average of 2.9%), and *Psophosphaera* (average of 2.5%) are still very low in abundance. Angiosperm pollen increases in both diversity and abundance, with the appearance of *Tricolporopollenites* sp., *Tricolpopollenites* sp., *Cranwellia* sp., *Proteacidites* sp., *Myrtaceidites* sp., *Quantonenpollenites* sp., and sporadic *Symplocospollenites* sp.

PA III: *Schizaeoisporites–Classopollis–Lytharites* (336.0–232.5 m). Compared with PA I and II, the palynoflora shows obvious changes. The pteridophyte spore content (25.9–75.5%, with an average of 49.9%) is greater than the content of the gymnosperm pollen (21.1–74.2%, with an average of 48.2%), whereas the angiosperm pollen abundance (0–4.4%, with an average of 2.0%) is slightly less. *Schizaeoisporites* are abundant, with an average of 21.8%, which is approximately twice the amount in PA II. For several ringed spores (*Polycingulatisporites* sp., *Foraminisporis* sp., *Nevesisporites* sp., and *Yichangsporites* sp.), the content is subordinate and represents 9.4% of this assemblage. The assemblage contains approximately 2.6% of *Laevigatosporites*. Other

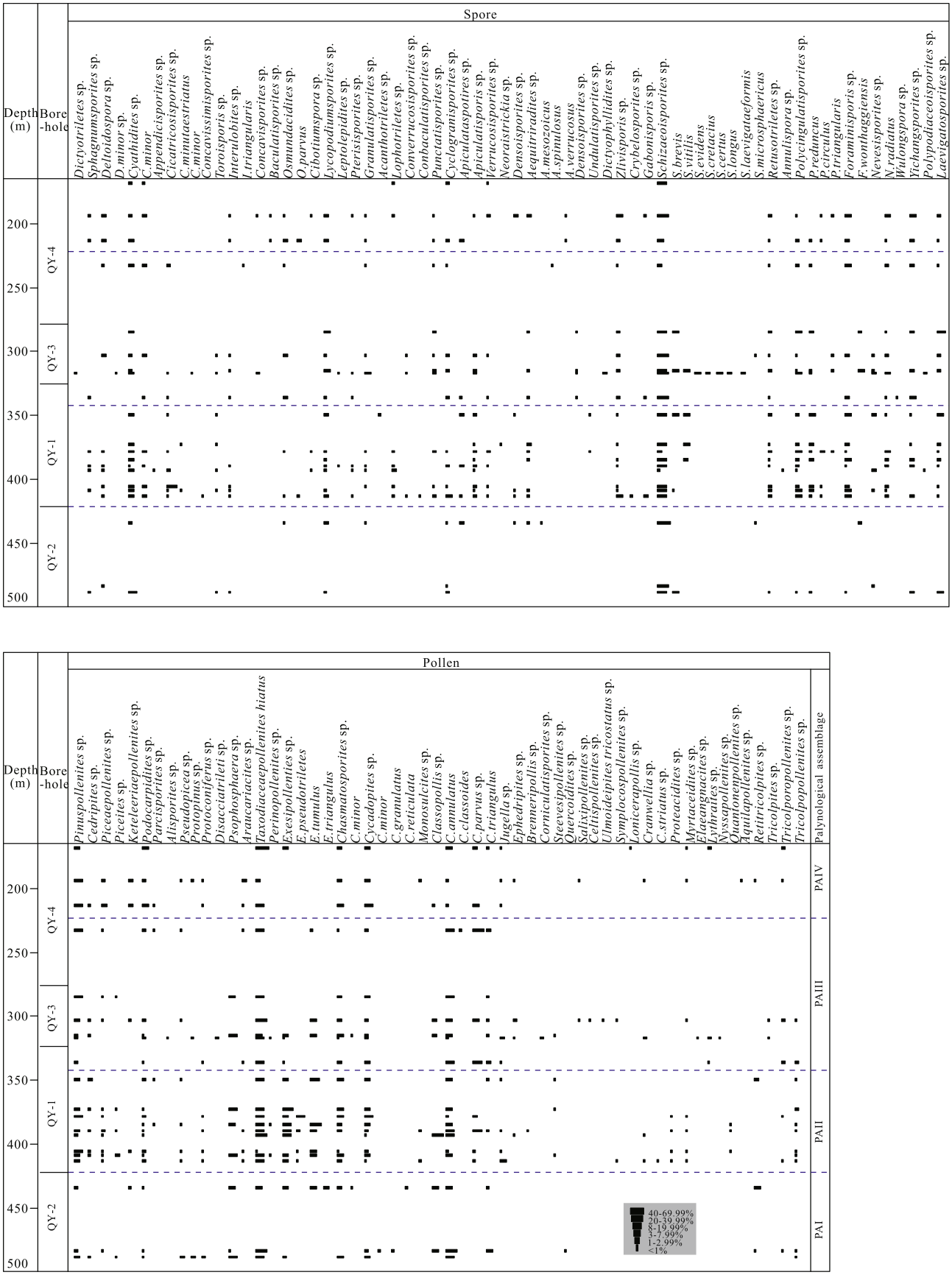

Fig. 4. Quantitative stratigraphic distribution of the spores and pollen recovered from the QY-1, QY-2, QY-3, and QY-4 boreholes in the Qianjiadian district, Kailu depression.

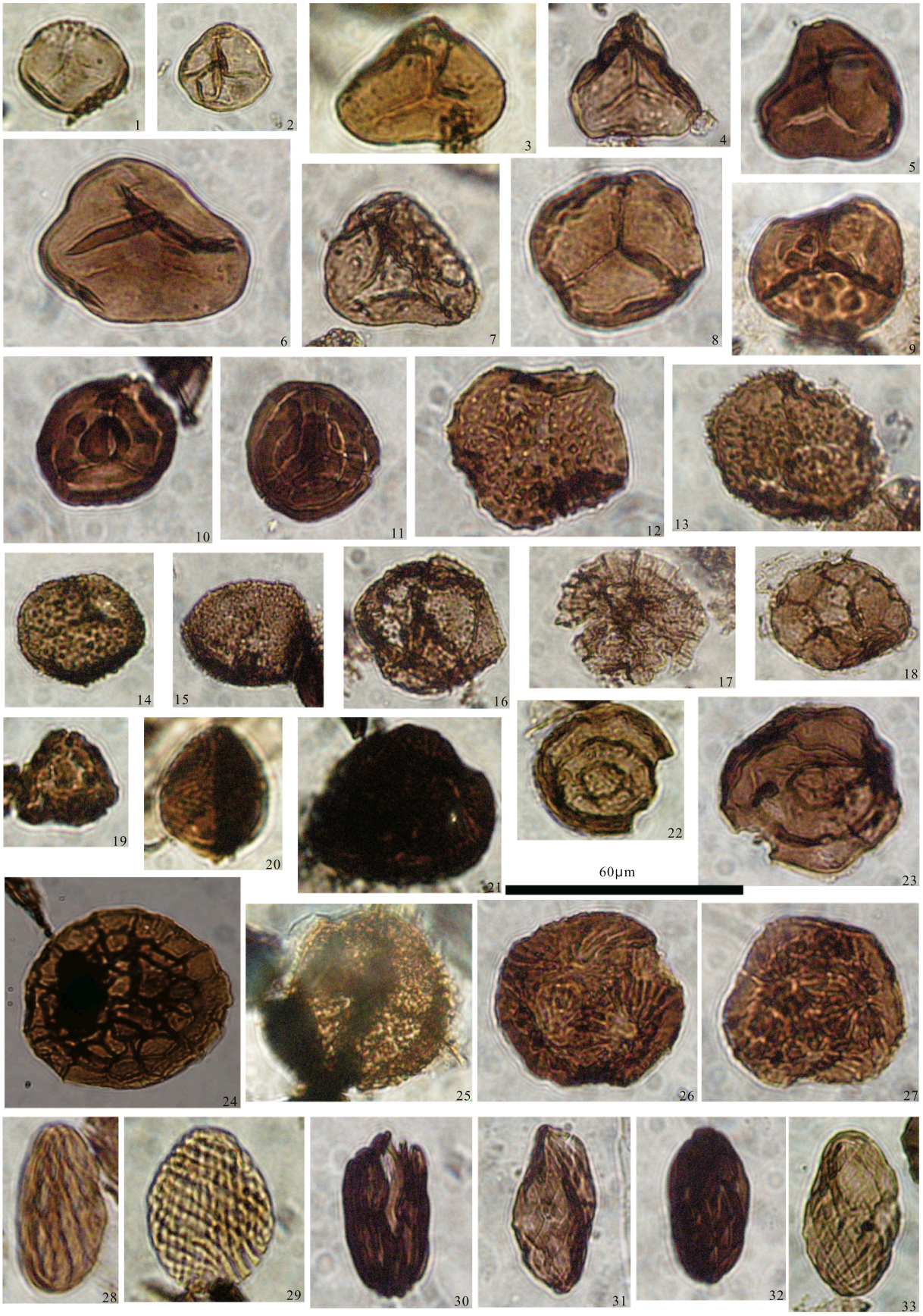

(caption on next page)

Fig. 5. Examples of the representative spore and pollen taxa recovered from the QY-1, QY-2, QY-3, and QY-4 boreholes. The scale bar is 60 μm. 1. *Sphagnumsporites* sp., 193.6 m, QY-4; 2. *Sphagnumsporites* sp., 488.5 m, QY-2; 3. *Deltoidospora* sp., 378.4 m, QY-1; 4. *Deltoidospora* sp., 213.5 m, QY-4; 5. *Cyathidites* minor, 303.0 m, QY-3; 6.*Cyathidites* sp., 303.0 m, QY-3; 7. *Cyathidites* sp., 213.5 m, QY-4; 8. *Retusotriletes* sp., 303.0 m, QY-3; 9. *Interulobites* sp., 303.0 m, QY-3; 10. *Polycingulatisporites* sp., 303.0 m, QY-3; 11. *Polycingulatisporites triangularis*, 303.0 m, QY-3; 12. *Foraminisporis* sp., 303.0 m, QY-3; 13. *Foraminisporis* sp., 193.6 m, QY-4; 14. *Osmundacidites parvus*, 213.5 m, QY-4; 15. *Osmundacidites parvus*, 213.5 m, QY-4; 16. *Osmundacidites* sp., 213.5 m, QY-4; 17. *Lycopodiumsporites* sp., 193.6 m, QY-4; 18. *Lycopodiumsporites* sp., 193.6 m, QY-4; 19. *Pterisisporites* sp., 413.2 m, QY-1; 20. *Cicatricosisporites* sp., 405.9 m, QY-1; 21. *Cicatricosisporites* sp., 232.5 m, QY-4; 22. *Yichangsporites* sp., 336.0 m, QY-1; 23. *Yichangsporites* sp., 315.0 m, QY-3; 24. *Zlivisporis* sp., 336.0 m, QY-1; 25. *Aequitriradites verrucosus,* 193.6 m, QY-4; 26. *Nevesisporites radiatus* 303.0 m, QY-3; 27. *Nevesisporites radiates*, 349.5 m, QY-1; 28. *Schizaeoisporites* sp., 336.0 m, QY-1; 29. *Schizaeoisporites* sp., 336.0 m, QY-1; 30. *Schizaeoisporites* sp., 303.0 m, QY-3; 31. *Schizaeoisporites* sp., 303.0 m, QY-3; 32. *Schizaeoisporites* sp., 160.6 m, QY-4; 33. *Schizaeoisporites* sp., 434.0 m, QY-2.

spores, such as *Cyathidites* sp., *Lycopodiumsporites* sp., *Punctatisporites* sp., and *Zlivisporis* sp., are also common. In the gymnosperm pollen, *Taxodiaceaepollenites hiatus* is characterized by a decrease in abundance compared with PA II, but it remains the major type at approximately 12.7%. *Classopollis* (Cheirolepidiaceae) content is slightly higher than the content in PA II, with abundances of 16.2%. We observe a slight increase in the bisaccate conifer pollen abundance, such as *Pinuspollenites* and *Podocarpidites,* which reaches, on average, 8.1%. In contrast, *Exesipollenties* were characterized by a marked decline in abundance, with an average of 2.9%. *Chasmatosporites, Cycadopites,* and *Psophosphaera* are still common in the PA III and do not vary significantly. Other common types include *Jugella* and *Ephedripites*. Tricolpates (or tricolporate) dominate the angiosperm pollen, as well as more diverse angiosperm types, while *Tricolporopollenites* are the most abundant. Other types are sporadic, including *Salixipollenites* sp., *Celtispollenites* sp., *Symplocospollenites* sp., *Cranwellia* sp., *Myrtaceidites* sp., *Elaeangnacites* sp., *Lythraites* sp., *Nyssapollenites* sp., and *Tricolporopollenites* sp.

PA IV: *Biasccate–Taxodiaceaepollenites–Aquilapollenites* (213.5–160.6 m). For PA IV, the gymnosperm pollen content (25.0–72.5%, with an average of 56.1%) is significantly higher than the pteridophyte spore content (22.5–70.7%, with an average of 40.8%), whereas angiosperm pollen content is less abundant (0–5.0%, with an average of 3.1%). For the pteridophyte spores, *Schizaeoisporites* (Schizaeceae) are again dominant, with an average of 16.2%. The ringed spore content (*Polycycliculasporites* sp., *Foraminisporis* sp., *Nevesisporites* sp., and *Yichangsporites* sp.) is subordinate and represents 7.5% of the total assemblage. Certain amounts of *Cyathidites* sp., *Granulatisporites* sp., *Punctatisporites* sp., *Leptolepidites* sp., and *Deltoidospora* sp., also occur and are continuously distributed throughout the samples, whereas other spores occur only sporadically. A sharp increase in the abundance of bisaccate conifer pollen (*Pinuspollenites* sp., *Cedripites* sp., *Piceaepollenites* sp., and *Podocarpidites* sp.) from 8.1% to 19.2% occurs in the PA IV. *Taxodiaceaepollenites hiatus* also increases in abundance from 12.7% to 21.1%. The *Classopollis* (Cheirolepidiaceae) content is characterized by a rapid decrease (5.8%) compared with the PA III. Other common taxa, including *Chasmatosporites* sp., *Cycadopites* sp., and *Exesipollenties* sp., are rare in PA IV and show slight changes compared with the previous assemblages. Angiosperm pollen increases in abundance and diversity, including *Tricoloporpollenites* sp., *Salixipollenites* sp., *Lonicerapollis* sp., *Myrtaceidites* sp., *Retitricolpites* sp., *Lythraites* sp., *Cranwellia* sp., and *Aquilapollenites* sp.

5. Discussion

5.1. Biostratigraphic information

Taxa with stratigraphic significance are generally lacking in our samples. Therefore, determining the sedimentary sequence age is more difficult, but still provides significant biostratigraphic information. *Classopllis* flourish in the Jurassic and play an important role in the Cretaceous. Other taxa, such as *Cicatricosisporites* sp., *Polycingulatisporites* sp., *Foraminisporis* sp., *Schizaeoisporites* sp., *Pterisisporites* sp., *Laevigatosporites* sp., *Concavissimisporites* sp., *Zlivisporis* sp., *Nevesisporites* sp., *Gabonisporis* sp., *Yichangsporites* sp., *Wulongspora* sp., *Exesipollenites* sp., and *Cranwellia* sp., are relatively common and important in the Cretaceous.

For the pteridophyte spores, *Schizaeoisporites* are the most prosperous species from the late Early Cretaceous to the early Late Cretaceous and are characterized by high abundances in the Early and Middle Cretaceous in China (Gao et al., 1999; Song, 1986). This is especially true in the case of *Schizaeoisporites. vitilis*, which generally occurs in Cenomanian–Santonian aged sediments (Bolchovitina, 1967). In addition, *Nevesisporites radiatus* is a common species during the Late Cretaceous in Russia, North America, and China. *Interulobites* are also an important species between the late Early Cretaceous and the early Late Cretaceous in the eastern United States (Stover, 1963). For the gymnosperm pollen, *Steevesipollenites* commonly appear in Cenomanian–Turonian aged sediments in West Africa, whereas no records have been found in pre-Cretaceous sediments (Zhu et al., 2012). *Exesipollenites* and *Classopllis* are common in the Late Cretaceous in China, but become scattered in the Paleogene (Li et al., 2008). As noted above, we assigned a Cretaceous age to the sedimentary sequence.

Angiosperm pollen plays an important role in the division and comparison of Cretaceous and subsequent strata (Doyle, 1969; Muller, 2010; Norris et al., 1975). In the PA I, angiosperm pollen is scarce and monotone. *Tricolpopollenites* are a small individual, whereas *tricolporopollenites* are always present as a medium-sized individual. Based on previous studies, *tricolporopollenites* usually appear in the late Albian or Cenomanian and might occur later than the *Tricolpopollenites* (Zhang, 1999). Associations between *Schizaeoisporites*, *Classopllis*, and common *tricolporopollenites* suggest that there is a good correlation with the SK 1 assemblage (i.e., a coring program at the Daqing Oilfield), which indicates that the geological age of PA I is likely late Turonian. In the PA II, *Proteacidites* and *Nyssapollenites* accompany the appearance of *Cranwellia*, which represents angiosperm pollen evolution to the *Cranwellia* stage in China and corresponds to the Turonian (Zhang, 1999). *Cranwellia* are an important, global Late Cretaceous taxon (Brenner, 1967; Dettmann, 1973; Laing, 1975). *Cranwellia* first occur in the upper Member of the Kukebai Formation in the Tarim Basin and the Qingshankou Formation in the Songliao Basin, which corresponds to the Turonian (Zhang, 1989; Zhang and Zhan, 1991) and the late Turonian–Coniacian, respectively (Li et al., 2011; Wan et al., 2013). Known as *Cranwellia striatella*, it first appears during the (late) Turonian from Siberian Russia to the Far East (Markevitch, 1994). This implies a late Turonian–Coniacian age range for the PA II. In the PA III, the appearance of *Lytharites*, along with other angiosperm pollen, such as *Cranwellia*, *Myrtaceidites*, and *Nyssapollenites*, indicates that the angiosperm pollen evolved into the *Lytharites–xinjiangpollis* stage in China, which corresponds to the Coniacian–Santonian (Zhang, 1999). *Lytharites* commonly appear in Coniacian deposits throughout the Tarim and Songliao Basin (Li et al., 2011; Wan et al., 2013). Thus, the age of the PA III is restricted to the Coniacian–Santonian. The PA IV is characterized by the inception of triprojectate pollen, i.e., the *Aquilapollenites. Aquilapollenites* flourished globally in the Late Cretaceous, as well

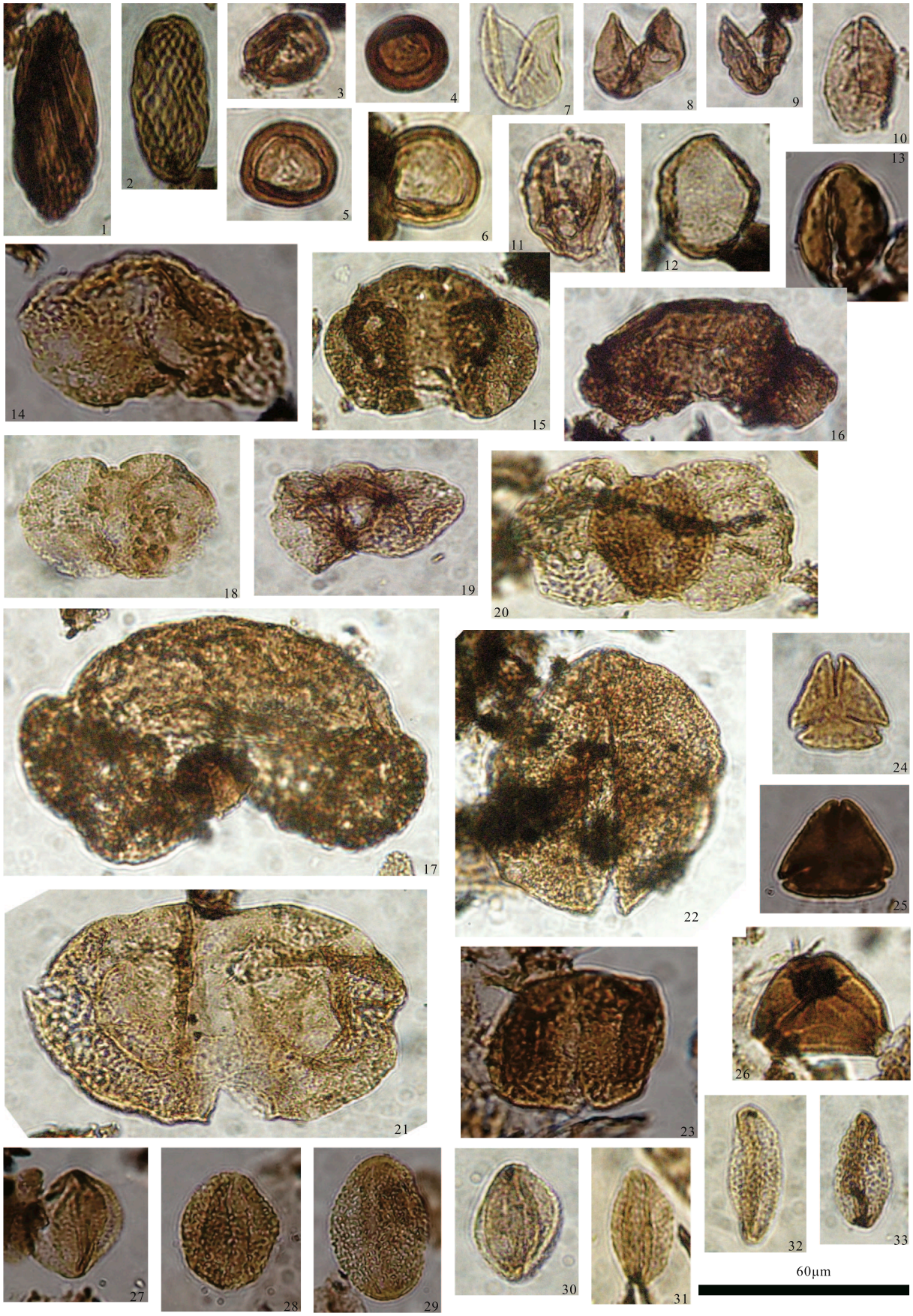

(caption on next page)

Fig. 6. Further examples of the representative spore and pollen taxa recovered from the QY-1, QY-2, QY-3, and QY-4 boreholes. The scale bar is 60 μm. 1. *Schizaeoisporites* sp., 434.0 m, QY-2; 2. *Schizaeoisporites* sp., 434.0 m, QY-2; 3. *Classopollis* sp., 160.6 m, QY-4; 4. *Classopollis annulatus,* 389.7 m, QY-1; 5. *Classopollis annulatus* 389.7 m, QY-1; 6. *Classopollis annulatus* 389.7 m, QY-1; 7. *Taxodiaceaepollenites hiatus* 413.2 m, QY-1; 8. *Taxodiaceaepollenites hiatus* 303.0 m, QY-3; 9. *Taxodiaceaepollenites hiatus* 483.5 m, QY-2; 10. *Chasmatosporites* sp., 378.4 m, QY-1; 11. *Chasmatosporites* sp., 349.5 m, QY-1; 12. *Cycadopites* sp., 378.4 m, QY-1; 13. *Cycadopites* sp., 213.5 m, QY-4; 14. *Pinuspollenites* sp., 378.4 m, QY-1; 15. *Pinuspollenites* sp., 213.5 m, QY-4; 16. *Pinuspollenites* sp., 303.0 m, QY-3; 17. *Keteleeriae pollenites* sp., 193.6 m, QY-4; 18. *Podocarpidites* sp., 336.0 m, QY-1; 19. *Podocarpidites* sp., 303.0 m, QY-3; 20. *Podocarpidites* sp., 213.5 m, QY-4; 21. *Protopinus* sp., 488.5 m, QY-2; 22. *Protoconiferus* sp., 303.0 m, QY-3; 23. *Parcisporites* sp., 349.5 m, QY-1; 24. *Tricolporopollenites* sp., 336.0 m, QY-1; 25. *Tricolporopollenites* sp., 336.0 m, QY-1; 26. *Lythraites* sp., 336.0 m, QY-1; 27. *Retitricolpites* sp., 349.5 m, QY-1; 28. *Retitricolpites* sp., 349.5 m, QY-1; 29. *Retitricolpites* sp., 349.5 m, QY-1; 30. *Retitricolpites* sp., 193.6 m, QY-4; 31. *Retitricolpites* sp., 434.0 m, QY-2; 32. *Retitricolpites* sp., 434.0 m, QY-2; 33. *Retitricolpites* sp., 434.0 m, QY-2.

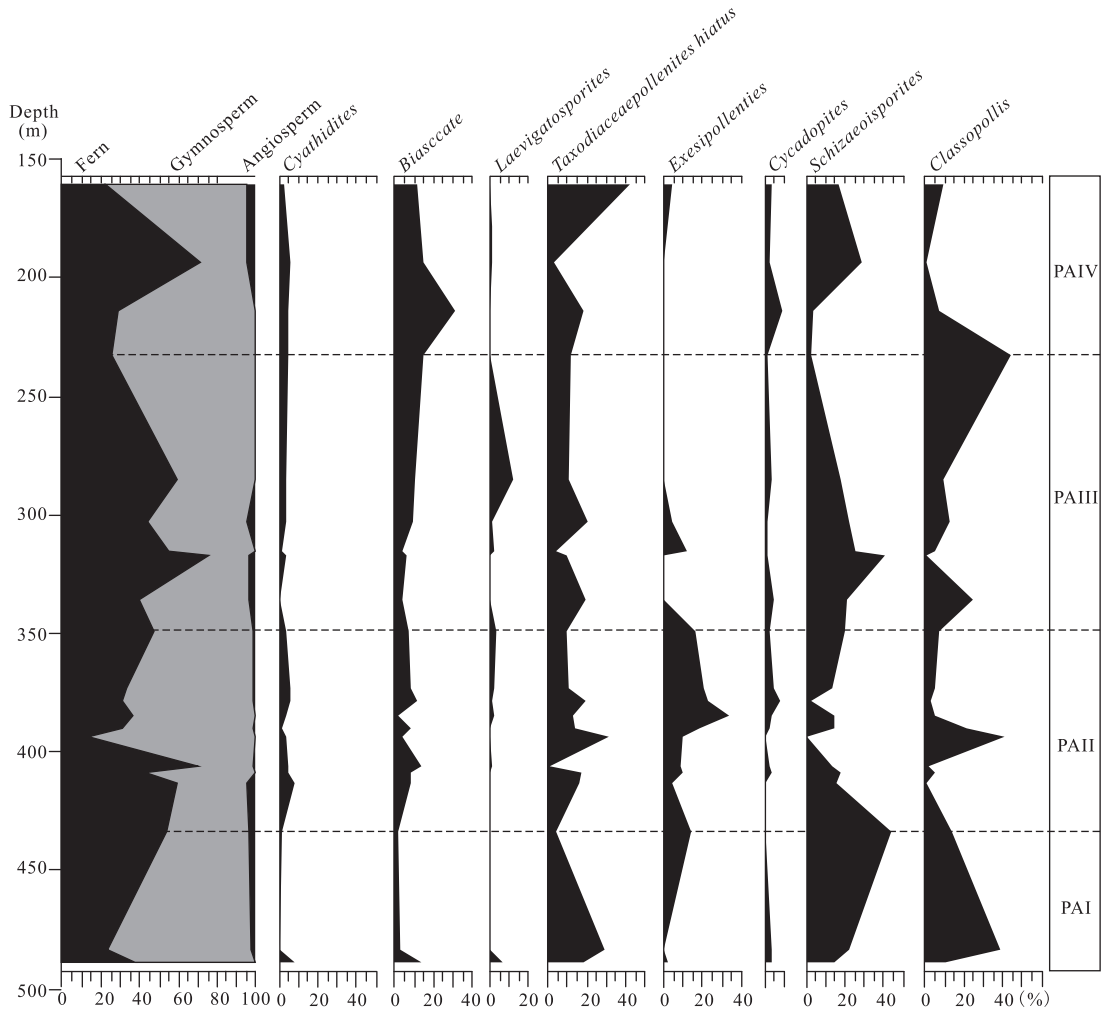

Fig. 7. A percentage sporopollen diagram of the selected sporomorph taxa observed in the QY-1, QY-2, QY-3, and QY-4 composite cores from the Qianjiadian district, Kailu depression.

as throughout the Pacific Rim. *Aquilapollenites* were common in the Santonian–Maastrichtian but became extinct at the end of the Late Cretaceous and were a relict in the Eocene. *Aquilapollenites* are comparable with other Late Cretaceous taxa distributed globally. Several previous studies examined *Aquilapollenites* in eastern Siberia, Japan, the northern United States, and China (Batten, 1984; Chlonova, 1961; Gao and He, 1992; Li et al., 2011; Nichols and Jacobson, 1982; Nichols et al., 2006; Samoilovich, 1967; Zhang, 1981). Nichols and Jacobson (1982) proposed that *Aquilapollenites* initiated in the earliest Campanian sediments in the Rocky Mountains of Utah and Wyoming. Nichols and Sweet (1993) summarized the geological record of *Aquilapollenites* and proposed that its first occurrence was at the Santonian–Campanian transition. Braman (2001) analyzed various triprojectate pollen assemblages from late Santonian sediments in Southern Alberta, Canada, and suggested that the initial occurrence of *Aquilapollenites* was in the early Santonian. However, through a comprehensive analysis of the SK 1 PAs, Li et al. (2011) suggested that the inception of *Aquilapollenites* is earlier for the Campanian Nenjiang Formation. Thus, the PA IV has an early Campanian age.

Based on the typical sporopollen species contained within the various assemblages, the sedimentary sequences range in age from the late Turonian to the early Campanian. These ages are comparable with the Qingshankou-Nenjiang Formations PAs from the SK 1.

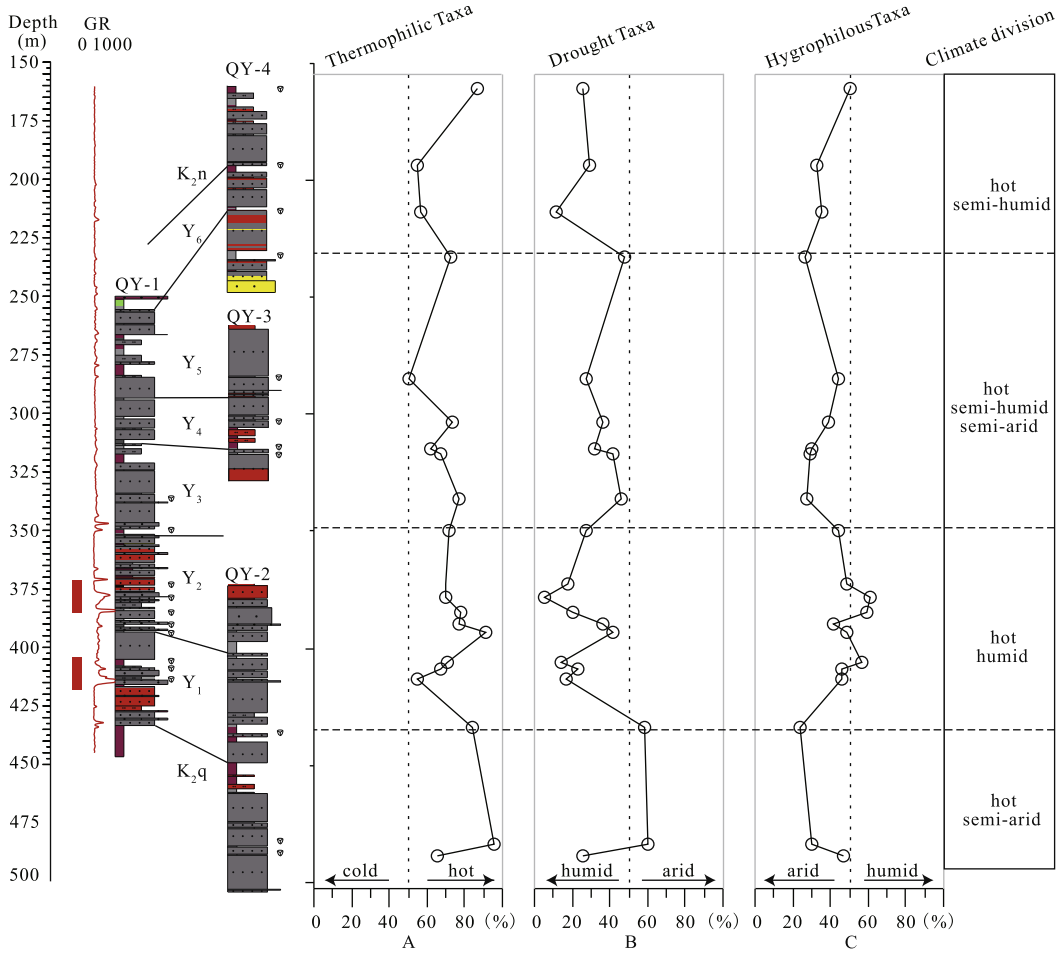

Fig. 8. The climate division and content variation between (A) thermophilic taxa, (B) drought taxa, and (C) hygrophilous taxa in the QY-1, QY-2, QY-3, and QY-4 composite cores from the Qianjiadian district, Kailu depression.

5.2. Palynoflora and paleoclimatic change

In the integrated body of the Earth's biosphere, biology and environment are both interdependent and mutually restrictive. A certain fossil assemblage represents a community and reflects that community's paleogeography, paleoclimate, and sedimentary environment (Wang et al., 2005a). Sporopollen fossils are plant products and vegetation is particularly sensitive to changes in climatic conditions. Changes in the diversity and abundance of sporopollen fossils are indicators of changes in the climate and environment. Most fossils have certain relationships with their parental plant, except for a few morphologic species whose genetic relationships remain unclear. To reconstruct past climate and environmental conditions in the Qianjiadian area, we compare the fossil pollen with their nearest living relatives in modern pollen assemblages that have well-defined ecological characteristics. This technique can be used to infer the regional paleoclimate.

Most fern spores prefer a shady and humid habitat (Cittert, 2002). For example, Cyatheaceae (*Cyathidites*) usually grow in tropical and sub-tropical humid valleys, along riverbanks of low altitude areas. Schizaeaceae (*Schizaeaceae*) are vegetation that grow in barren soil and prefer hot and arid environments in the southern hemisphere and equatorial regions. Polypodiaceae (*Laevigatosporites*) are widely distributed in subtropic and temperate areas, generally growing in hot and humid environments (Palynology Team, Institute of Botany, Academia, 1976). The predominant coniferous forest of gymnosperm pollen are known from a wide ecological range. Pinaceae (*Piceaepollenites*, *Cedripites*, *Abiespollenite,* and *Tsugapollenites*) and other conifer types are mostly distributed in sub-alpine areas, characterized by cool climatic conditions (Wang et al., 2005b). Cupressaceae (*Exesipollenites*) usually grow in temperate areas and are typical hygrophilous plants. Taxodiaceae conifers (*Taxodiaceaepollenites*) inhabit humid lowlands and colder environments (Pelzer et al., 1992). Cheirolepidiaceae (as indicated by *Classopollis*) are a common Mesozoic plant group that spread from hot, equatorial regions to warm, high-latitude areas, where the typical dwarf coniferophyte adapted to arid conditions (Vakhrameyev, 1982). In addition, these drought-tolerant trees or shrubs are accustomed to highland slopes, lowland coasts, and saline-alkaline environments in areas with developed water systems (Heimhofer et al., 2008; Mendes et al., 2010; Vakhrameyev, 1982). Based on the climatic parameters of various sporopollen taxa, we discuss the flora and paleoclimate corresponding to the four PAs.

In PA I, the palynoflora is dominated by gymnosperms. Cheirolepidiaceae (*Classopollis*), which grow in dry and hot environments, account for the largest proportion of gymnosperms. The lowest abundance of bisaccates of pinaceous affinity, such as the Pinaceae and Podocarpaceae (including *Cedripites*, *Piceaepollenites*, *Pinuspollenites,*

Table 1
Synsedimentary paleoclimate in U-bearing rocks and their effects on large-scale epigenetic uranium mineralization throughout northern China. Data from Bonnetti et al. (2017), Cai et al. (2007a,b), Luo et al. (2007), Min et al. (2005a,b), and Wu (2005).

Basin	Songliao Basin		Ordos Basin		Tuha Basin	Yili Basin
	Qianjiadian Uranium deposit	Baixingtu Uranium deposit	Dongsheng Uranium deposit	Daying Uranium deposit	Shihongtan Uranium deposit	Wuyier Uranium deposit
Uranium-bearing horizon	Upper Cretaceous Yaojia Formation		Middle Jurassic Zhiluo Formation		Lower-Middle Jurassic Shuixigou Group	Lower-Middle Jurassic Shuixigou Group
Uranium-bearing lithology	Gray medium-to fine-grained sandstones		Gray medium-to fine-grained sandstones		Gray sandstone	Gray coarse-to medium-grained sandstones
Synsedimentary palaeoclimate	Huimd		Huimd		Huimd	Huimd
Mineralization age	E_{2-3}–N		K_1, K_2, N_1	E_3–N_2	K_1, E_{2-3}, N_1	K, N, Q_1

and *Podocarpidites*), indicates the presence of a hot and arid climate. Schizaeceae (*Schizaeoisporites*) grew in arid and hot conditions, which were dominated in the ferns. However, other ferns, which prefer warm and humid conditions, show extremely low abundances and differentiation (Fig. 7). This indicates a hotter, more arid climate. On the other hand, the percentages of thermophilic taxa, on average, have the highest values (81.7%), whereas the drought-tolerant and hygrophilous taxa total 48% and 33.5%, respectively (Fig. 8). The PA I composition indicates that the Kailu Depression experienced a hot and semi-arid tropical climate during this period.

Based on an obvious decrease in the pteridophytes (e.g., Schizaeceae) during this interval, the PA II turned towards a humid climate. The Cheirolepidiaceae abundance also significantly declines. The percentage of pinaceous pollen slightly increases compared with the PA I (Fig. 7). The low abundance of Schizaeceae and Cheirolepidiaceae indicates a warm and relatively humid climate during this period. In addition, the percentage of thermophilic taxa decreases to 72.3%, which indicates a decline in the temperature. The percentage of drought-tolerant taxa shows the lowest average value (22.4%), whereas the hygrophilous taxa increased to an average peak value (50.3%) (Fig. 8). These conditions imply that, during this period, the Kailu Depression was characterized by hot and humid climatic conditions.

In the PA III, there are significant changes in the palynoflora. This is characterized by the higher pteridophyte abundance compared with the gymnosperms. Simultaneously, the relatively high Schizaeceae abundance is the main cause for the increase in ferns. The thermophilic and hygrophilous pteridophytes still have a low abundance. The Cheirolepidiaceae abundance shows a gradual increase and reaches its peak values. The abundance of bisaccates of pinaceous affinity did not have any significant changes (Fig. 7). In addition, the percentage of thermophilic taxa remains a declining trend, with an average of approximately 67.3% (Fig. 8). The growth of drought-tolerant taxa from 22.4% to 38.3%, with declining hygrophilous taxa abundance (32.7%), indicate an increase in drought conditions. Overall, the Kailu Depression experienced a hot and semi-arid to semi-humid climate during this period.

In the PA IV, the bisaccate pollen-producing conifers show a significant growth in abundance and become the dominant plant type (Fig. 7). During the Late Cretaceous in northern China, this was the main vegetation element, which indicates a humid and colder climate (Batten, 1984; Brenner, 1976; Hochuli et al., 1999). The abundance of Cheirolepidiaceae and Schizaeceae, which was adapted to hot and arid conditions, gradually reduced, while the hygrocolous ferns were experienced no significant abundance fluctuations. Moreover, the percentage of the thermophilic taxa (65.9%) in the PA IV is slightly lower than the percentage in the PA III. The percentage of drought-tolerant taxa once again decreased to 22.1%, while the hygrophilous taxa increased to 39.6% (Fig. 8), indicating that there was a change in climate from previous conditions to semi-humid and hot subtropical conditions.

Overall, the palynoflora analyzed from the Kailu Depression indicates the presence of a hot subtropical climate during the late Turonian to early Campanian, although the temperature is characterized by a gradually decreasing trend. The paleoclimate of the synsedimentary Yaojia Formation was predominantly semi-humid, but also experienced semi-arid fluctuations.

5.3. Impact of paleoclimate evolution on uranium mineralization

Numerous previous studies have emphasized the importance that arid and semi-arid paleoclimatic conditions have on the genetic mechanism of sandstone-type uranium deposits (Jiao et al., 2015). During semi-arid and arid climatic conditions, rocks experience intense physical weathering. Then, large amounts of uranium leach out, infiltrate into the groundwater, and migrate over long distances as stable uranyl ions. Both poorly developed vegetation and low clay mineral abundance, a consequence of the semi-arid to arid climate, contribute to

oxygen infiltration with precipitation and avoid uranium loss during transport from the orogenic belt to the sedimentary basin. Because evaporation is greater than precipitation, the uranium concentration in groundwater is elevated. However, through a comparison of sandstone-type uranium deposits from different regions and ages in northern China, we suggest that the synsedimentary paleoclimate in uranium-bearing rocks plays a more important role during uranium mineralization. For instance, the paleoclimate restricted not only the development of potential sandstone but also the type, abundance, and distribution of reduced materials within uranium-bearing rocks. The close association between the synsedimentary paleoclimate conditions and several structural factors, such as the orogenic belt source area uplift, the slope's hydraulic gradient, and the discharge area during the metallogenic epoch, control the size, morphology, and spatial orientation of the sandstone-type uranium deposits.

5.3.1. Humid synsedimentary paleoclimate controls on U-bearing rocks

Gray/gray–black (or coal-bearing) continental clastic rocks related to a humid environment have significant metallogenic implications as these confined permeable sandstones preserve abundant organic matter and pyrite (Casagrande, 1987; Diessel, 1992). These clastic rocks are good reservoirs for the sandstone-type uranium deposits. When in contact with oxygenated water, U (IV) is oxidized and infiltrated into groundwater as U (VI) ions. When it encountered the gray/gray–black reduced sandstones, U (VI) ions may be trapped by organic matter (Owen and Otton, 1995), reduced and precipitated. Thus, reduced sandstones, which are deposited in a humid environment, may provide significant geochemical reducing barriers and control the sandstone-type uranium mineralization.

Uranium-bearing rocks throughout the Qianjiadian area in the Songliao Basin are coarse to very fine-grained braided channel sandstones derived from the Yaojia Formation (Fig. 8). PAs suggest that the Yaojia Formation U-bearing rocks were mainly deposited in a humid environment. Similar climatic conditions were identified in U-bearing rocks from other sandstone-type uranium deposits throughout northern China (Table 1), such as the Shuixigou Group (including the Badaowan, Sangonghe, Xishanyao, and Toutunhe Formations) in the Junggar (Yang and He, 2016), Tuha, and Yili Basins (Chen et al., 2011; Wu, 2005), and the Zhiluo Formation in the Ordos Basin (Sun et al., 2017). The sandstone-type uranium mineralization has been generally attributed to U (VI) reduction via sulfide and organic matter during low-temperature conditions (Granger and Warren, 1969; Rackley, 1972; Reynolds et al., 1982). The formation of organic matter contributes to the presence of a humid climate, which is an indicator for future U exploration.

5.3.2. Uranium metallogenic model

The uranium mineralization of the Qianjiadian deposit is hosted in the reduced sandstones of the Yaojia Formation. During the Yaojia Formation deposition, U-rich basement rocks, such as the Precambrian gneiss, some Paleozoic to Mesozoic granites, or Late Jurassic felsic volcanic rocks (Zhang et al., 2010; Wu et al., 2011; Li et al., 2012; Zhou et al., 2012; Bonnetti et al., 2017), were weathered, denuded, and transported to the sedimentary basin, which could have provided a potential source for uranium concentration and its subsequent mineralization.

A humid climate during the deposition of the Yaojia Formation was responsible for abundant and evenly distributed reducing materials in the sandstones. Based on regional petrological observations and the QY-1, QY-2, QY-3, and QY-4 drill cores (Fig. 8), the Yaojia Formation was characterized by gray to purple–red clastic sediments that consisted of pebbly coarse sands and medium–coarse sandstones, which provided channels for fluid migration and suitable reservoirs for uranium. Large amounts of carbonaceous clastics and pyrite, which are related to the humid climate and preserved in these sandstones, are useful for the uranium pre-concentration and providing significant geochemical reducing barriers for epigenetic uranium mineralization.

The Songliao Basin entered a stage of structural inversion at the end of the Late Cretaceous (Li et al., 2012), which resulted in the continuous structural uplift of the study area. Simultaneously, uranium leached out from outcropping source rocks and infiltrated into oxygenated waters. The uplift and tilt of the strata allowed the oxygenated waters to infiltrate into the strata. Then, during the main mineralization stage, the activated U (VI) were carried through the permeable sandstones by oxidizing water to the redox interface where the precipitation of uranium occurred. Tectonic uplift continued from the Late Cretaceous to the Neogene (Cheng et al., 2018), which corresponds with the timing of the uranium mineralization in the Baixingtu (76–20 Ma; Bonnetti et al., 2017) and Qianjiadian deposits (43–28 Ma and 19–3 Ma; Zhao et al., 2018, under revision after first review).

The sandstone-type uranium deposits formed via a combination of multiple factors, in which the humid paleoclimate was an essential condition that induced uranium mineralization. The humid climate was responsible for reduced sandstone formation and uranium pre-concentration, which provided the conditions for the epigenetic uranium mineralization.

6. Conclusions

Based on analyses of the PAs, recovered from the QY-1, QY-2, QY-3, and QY-4 boreholes in the Kailu Depression, northeastern Songliao Basin, we conclude that these successions are late Turonian to early Campanian in age. We reconstructed the palynoflora history and paleoclimate evolution in the Kailu Depression from the late Turonian to the early Campanian. The percentage of thermophilic taxa showed a gradually decreasing trend, but remained at a relatively high abundance, which indicates a hot tropical/subtropical climate. Based on cyclical fluctuations of the percentage of drought and hygrophilous taxa, the corresponding climate from assemblages PA I to PA IV were discussed as follows: the climate was semi-arid in the PA I, and changed to a humid environment in the PA II. Subsequently, the climate changed to semi-arid and semi-humid conditions in the PA III, with an increase in drought. Finally, the climate became humid once more in the PA IV. Uranium mineralization in this region requires a humid climate, which was responsible for reduced sandstone formation and uranium pre-concentration and provided favorable conditions for epigenetic uranium mineralization.

Acknowledgements

This work was supported by Projects 2015CB453000 of National Key Basic Research Program (973) and the Project 20160128 of China Geological Survey. We thank Sun Lixin, Sima Xianzhang for helps in the field expedition. We are grateful to Lu Huinan of the Nanjing Institute of Geology and Palaeontology, Chinese Academy of Sciences for his assistance with sample handing and fossil identification. We also thank two anonymous reviewers for their helpful comments and careful reviews.

Appendices

Table A1

Table A1
Statistics of sporopollen from the QY-1, QY-2, QY-3, and QY-4 boreholls.

Boreholls	QY-4				QY-3				QY-1										QY-2		
Fossils	Depth (m)																				
	168.6	193.6	226.5	232.5	284.8	303	315	317	336	349.5	372.8	378.4	384.6	389.7	393.2	405.9	408.5	413.2	434	483.5	488.5
Dictyotriletes sp.								0.28													
Sphagnumsporites sp.		0.86							0.43			0.77		0.29	0.31		0.58				0.61
Deltoidospora sp.		1.44	4.55	0.62		1.69						0.77		0.15	0.62	0.99		0.32		0.30	
D. minor								0.28													
Cyathidites sp.	1.67	2.87	40.91	3.69	3.83	2.11	1.87	4.23		3.44	5.56	3.46	3.19	0.73	3.74	3.29	5.19	6.33	1.77		8.54
C. minor	0.83	2.59		1.23		1.27			0.43			2.88		0.29		1.64		1.90			
C. australis			7.95																		
Appendicisporites sp.															0.31						
Cicatricosisporites sp.				2.15				0.56	0.43	0.34		0.58			1.25	32.57	0.29	0.16			
C. minutaestriatus sp.											0.33						0.86				
C. minor								0.56													
Concavissimisporites sp.																		0.32			
Reticulatisporites sp.			1.14																		
Toroisporis sp.						0.63		0.56		0.69	0.33				0.31		0.58				0.61
Interulobites sp.		0.86				0.21	0.53		0.43					0.73		0.66	0.29	0.95			0.91
I. triangularis				0.62																	
Concavisporites sp.		0.29	1.14					1.13													
Baculatisporites sp.		0.86																			
Osmundacidites sp.		0.29		0.62		1.48			1.51			0.58						0.32	0.88		
O. parvus																		0.63			
Cibotiumspora sp.		0.57										0.19			0.31						
Lycopodiumsporites sp.		2.59			6.70	0.84	4.28		0.22	1.03		0.38	0.21	0.44	0.31		0.58	1.27	1.33		0.61
Leptolepidites sp.			2.27					0.85						0.15							
Pterisisporites sp.		0.29						0.85	0.22					0.15	0.31			0.47			
Granulatisporites sp.		0.57		0.31		0.63		4.79				0.38		0.58	0.31	0.66			0.88		
Acanthotriletes sp.										0.34											
Lophotriletes sp.	0.83	0.57										0.58		0.44	1.56	0.33		0.95			
Converrucosisporites sp.			9.09			0.84		0.28										0.63			
Conbaculatisporites sp.																		0.47			
Punctatisporites sp.		0.29	3.41	0.31	1.91	0.42	2.67	1.69				1.54				0.66		2.06			
Cyclogranisporites sp.	1.67			0.92		2.11	1.60		1.72			0.77		1.31		0.66		3.32	0.44	0.30	1.22
Apiculataspotires sp.									0.43	1.72				1.31				0.32	1.33		
Apiculatisporis sp.		0.57	3.41			1.90	1.87	1.69		1.03	0.65	1.15	0.21	1.17	0.31	1.32	0.58	1.90			
Verrucosisporites sp.	0.83	1.15				0.42			0.43			1.15		0.58		0.66		0.32			
Neoraistrickia sp.											0.33										
Densoisporites sp.		1.15								0.69							0.58	0.16	0.44		
Aequitriradites sp.		1.44			0.96		0.80		0.22		1.31	0.19	0.64				0.86	0.16	0.44		
A. mesozoicus																			0.44		
A. spinulosus				0.62																	
A. verrucosus		0.29																			
Densoisporites sp.					0.96		0.27														
Densosporites sp.								0.28	0.43												
Undulatisporites sp.										0.34		0.19									
Dictyophyllidites sp.								1.13													
Zlivisporis sp.		4.02		0.92	1.91	1.90	1.87		2.15	0.69	0.65		0.43	0.44		0.66	0.86	3.16			

(*continued on next page*)

Table A1 (*continued*)

Boreholls	QY-4				QY-3				QY-1										QY-2		
Fossils	Depth (m)																				
	168.6	193.6	226.5	232.5	284.8	303	315	317	336	349.5	372.8	378.4	384.6	389.7	393.2	405.9	408.5	413.2	434	483.5	488.5
Crybelosporites sp.																		0.16			
Gabonisporis sp.		0.86							0.22									1.42			
Schizaeoisporites sp.	16.67	28.45		2.77	13.88	20.89	16.04	27.89	21.29	11.00	10.13	2.31	12.77	14.43	0.62	13.16	17.29	15.66	43.81	22.09	10.98
S. brevis					4.31		5.35			6.19							0.86				3.35
S. vitilis							4.55			3.09	3.27		2.34								
S. evidens			2.27					3.66													
S. cretacius								1.13													
S. certus								3.66													
S. longus								1.97													
S. laevigataeformis								2.54													
S. microsphaericus						0.84													0.44		
Retusotriletes sp.		1.44		0.31	1.44	0.63	2.67		0.43	1.37	0.98	1.73	0.64	0.73		2.30	2.31	1.58			0.61
Annulispora sp.															0.62						
Polycingulatisporites sp.		0.57		1.54	4.31	0.84	0.53	5.07		2.75	2.94	4.23	1.91	2.62	0.93	1.97	3.46	4.75			0.61
P. reduncus				0.62	2.87		0.80	0.85		3.09	1.96	0.77	2.55			1.32	2.59	0.32			0.30
P. circulus		0.57										1.15				0.66		0.63			
P. triangularis		0.86				0.42	0.27					0.38									
Foraminisporis sp.		5.46		5.85		1.48			1.08	3.78	1.31	0.38	4.47	0.73		2.96	3.75	4.43			0.61
F. wonthaggiensis					1.44		3.48												1.33		
Nevesisporites sp.						0.42	0.53	2.25		1.03					1.25		0.58			0.30	
N. radiatus		4.60		1.23	0.96	1.27		5.07	0.65	0.34		3.08	2.98	1.46		2.63	0.86	2.85			
Wulongspora sp.									0.22												
Yichangsporites sp.		3.16		1.23	1.44		2.94		6.88	0.69	0.65		1.06	1.46				1.11			1.22
Polypodiaceoisporites sp.								2.25							0.31						
Laevigatosporites sp.		1.15		0.31	11.96	1.05	2.14			3.78	2.29	0.96	2.55	0.44		0.66		0.32			7.01
Pinuspollenites sp.	6.67	8.33		12.31	9.09	6.75	2.94	2.54	2.58	3.78	5.56	9.23		5.54	2.80	8.55	4.61	5.85	1.33	1.79	4.57
Cedripites sp.			9.09			0.21	0.53			1.03	0.33			0.44		0.33	0.29				0.91
Piceaepollenites sp.		2.01		0.62	0.48	0.63					0.33	0.38		1.02	0.31	0.66	0.86	0.32		0.30	
Piceites sp.					0.48						0.65			0.29			1.73				0.61
Keteleeriaepollenites		1.72				0.63										0.66			0.44		
Podocarpidites sp.	5.00	1.15	5.68	1.54		1.27	0.80	1.69	0.43	1.03	0.98	1.54	0.85	0.73	0.93	2.30	0.86	1.27	0.44	0.60	0.91
Parcisporites sp.				0.31						0.69			0.64								
Alisporites sp.								0.28													
Pseudopicea sp.		0.29		0.31		0.21				0.69			0.21			0.33		0.47			2.74
Protopinus sp.		0.29	1.14					0.28													1.22
P. latebrosa			1.14																		
Protoconiferus sp.		0.86							0.43			0.58		0.73		0.99		0.32			2.44
Disacciatrileti sp.								1.13													
Psophosphaera sp.					4.78		9.09				10.13		3.83				8.07		5.31	0.60	10.06
Araucariacites sp.		1.15		0.31					0.65					0.29		0.33		0.16			
Taxodiaceaepollenites hiatus	41.67	2.87		12.00	10.53	20.89	4.28	9.30	19.35	9.62	11.11	19.04	12.77	14.43	30.84	0.99	17.29	15.66	4.42	29.55	18.29
Perinopollenites sp.								0.28					0.64				0.86				
Exesipollenties sp.	4.17						5.61	0.28	0.22	7.22	20.92	7.12	12.77	11.66	9.66		3.17	3.80	4.42		2.74
E. pseudotriletes												15.38		2.33		0.99		0.79			
E. tumulus				0.31		4.01	6.68			9.28			21.06	4.08		7.24	6.34		4.87		
E. triangulus																			4.42		
Chasmatosporites sp.	1.67	1.15		0.62	2.87	1.48	7.22	0.56	2.58	7.22	5.56	3.65	1.91	2.04		0.66	3.46	1.42	2.21		3.05
C. minor							0.80												0.44		
Cycadopites sp.	3.33	3.16		1.23	3.83	1.05	1.07	1.97	4.73	3.09	5.23	8.46	3.83	2.19	0.62	2.30	3.75	0.79		2.69	3.96
C. minor																				0.90	
C. granulatus																				0.30	

(*continued on next page*)

Table A1 (*continued*)

Boreholls	QY-4				QY-3				QY-1										QY-2		
Fossils	Depth (m)																				
	168.6	193.6	226.5	232.5	284.8	303	315	317	336	349.5	372.8	378.4	384.6	389.7	393.2	405.9	408.5	413.2	434	483.5	488.5
C. reticulata																			0.88		
Monosulcites sp.		0.57												0.15				0.32			
Classopollis sp.			1.14			2.32	2.14								30.84				7.52	4.48	
C. major			1.14																		
C. annulatus	6.67	0.57		10.77	8.13	5.70	3.21	0.28	14.41	6.19	4.58	0.38	4.89	8.02	9.97	0.66	4.61		5.75	29.55	10.98
C. classoides				0.62																	
C. parvus	1.67			30.46		4.64			9.03			2.69		13.12		0.66		0.79			
C. triangulus	0.83			2.77	0.96	0.42	0.27		1.29	0.69				0.44					0.88	4.18	
Jugella sp.	0.83	0.57						1.13	0.65	0.34				0.29		0.66		4.43			
Ephedripites sp.		0.29				1.05									0.31						
Ephedripites sp.								0.28													
Brenneripollis sp.														0.15							
Corniculatisporites sp.			1.14					1.13													
Steevesipollenites sp.							0.27			0.34	0.65						0.29				
Quercoidites sp.																				0.90	
Salixipollenites sp.		0.86				0.21															
Celtispollenites sp.						0.21															
Ulmoideipites tricostatus						0.21															
Symplocospollenites sp.						0.21												0.32			
Lonicerapollis sp.	0.83																				
Cranwellia sp.		0.29						1.13							0.31			0.79			
C. striatus																		0.63			
Proteacidites sp.												0.19		0.58		0.66		0.95			
Myrtaceidites sp.	0.83	0.57				0.21						0.38		0.29		0.66		0.95			
Elaeangnacites sp.								0.28													
Lythraites sp.	1.67							1.41	0.22												
Nyssapollenites sp.								0.28													
Quantonenpollenites													0.21	0.15		0.33					
Aquilapollenites sp.		0.86																			
Retitricolpites sp.		0.86								1.03									3.10	0.60	
Tricolpites sp.			3.41			0.21		0.28													
Tricolporopollenites sp.	1.67	0.86				2.53			1.29			0.38						0.16		0.30	
Tricolpopollenites sp.						0.63			2.37	0.34	1.31		0.43	0.44		0.33	0.86	0.47		0.30	0.30

References

Abbink, O., Targarona, J., Brinkhuis, H., Visscher, H., 2001. Late Jurassic to earliest Cretaceous palaeoclimatic evolution of the southern North Sea. Global Planet. Change 30, 231–256.

Batten, D.J., 1984. Palynology, climate, and the development of Late Cretaceous floral provinces in the Northern Hemisphere; a review. In: Brenchley, P.J. (Ed.), Fossils and Climate. John Wiley and Sons Ltd, Chichester, pp. 127–164.

Bolchovitina, N.A., 1967. The fossil spores of the family Gleicheniaceae (morphology and taxonomy). Rev. Palaeobot. Palyno. 3, 59–64.

Bonnetti, C., Malartre, F., Huault, V., Cuney, M., Bourlange, S., Liu, X., Peng, Y., 2014. Sedimentology, stratigraphy and palynological occurrences of the late Cretaceous Erlian Formation, Erlian Basin, Inner Mongolia, People's Republic of China. Cretac. Res. 48, 177–192.

Bonnetti, C., Cuney, M., Malartre, F., Michels, R., Liu, X., Peng, Y., 2015. The Nuheting deposit, Erlian Basin, NE China: Synsedimentary to diagenetic uranium mineralization. Ore Geol. Rev. 69, 118–139.

Bonnetti, C., Liu, X.D., Yan, Z.B., Cuney, M., Michels, R., Malartre, F., Mercadier, J., Cai, J.F., 2017. Coupled uranium mineralisation and bacterial sulphate reduction for the genesis of the Baxingtu sandstone-hosted U deposit, SW Songliao Basin, NE China. Ore Geol. Rev. 82, 108–129.

Braman, D.R., 2001. Terrestrial palynomorphs of the upper santonian-? Lowest campanian milk river formation, Southern Alberta, Canada. Palynology 25, 57–107.

Brenner, G.J., 1967. Early angiosperm pollen differentiation in the albian to cenomanian deposits of delaware (U.S.A.). Rev. Palaeobot. Palyno. 1, 219–227.

Brenner, G.J., 1976. Middle Cretaceous floral provinces and early migrations of angiosperms. In: Beck, C.B. (Ed.), Origin and Early Evolution of Angiosperms. Columbia University Press, New York, pp. 23–47.

Cai, C., Li, H., Qin, M., Luo, X., Wang, F., Ou, G., 2007a. Biogenic and petroleum-related ore-forming processes in Dongsheng uranium deposit, NW China. Ore Geol. Rev. 32, 262–274.

Cai, C., Dong, H., Li, H., Xiao, X., Ou, G., Zhang, C., 2007b. Mineralogical and geochemical evidence for coupled bacterial uranium mineralization and hydrocarbon oxidation in the Shashagetai deposit, NW China. Chem. Geol. 236, 167–179.

Casagrande, D.J., 1987. Sulphur in peat and coal. In: Scott, A.C. (Ed.), Coal and Coal Bearing Strata: Recent Advances. Geol. Soc. London, Sp. Pub., pp. 87–105.

Chamberlain, C.P., Wan, X., Graham, S.A., Carroll, A.R., Doebbert, A.C., Sageman, B.B., Blisniuk, P., Kent-Corson, M.L., Wang, Z., Wang, C., 2013. Stable isotopic evidence for climate and basin evolution of the Late Cretaceous Songliao basin, China. Palaeogeogr. Palaeoclimatol. Palaeoecol. 385, 106–124.

Chen, P., Chang, Z., 1994. Nonmarine Cretaceous stratigraphy of eastern China. Cretac Res. 15, 245–257.

Chen, D., Liu, W., Jia, L., 2011. Paleo-climate evolution in China and its control on the metallization of sandstone type uranium deposit of Meso-Cenozoic basins. Uranium Geol. 27, 321–326 (in Chinese with English abstract).

Chen, F., Zhang, M., Lin, C., 2005. Sedimentary environments and uranium enrichment in the Yaojia Fm, Qianjiadian depression, Kailu Basin, Nei Mongol. Sediment. Tethy. Geol. 25, 74–79 (in Chinese with English abstract).

Cheng, X., 1982. Situation of Songliao Basin in the Plate tectonics and and its hydrocarbon occurrence. Petrol. Explor. Dev. 43–52 (in Chinese with English abstract).

Cheng, Y., Wang, S., Li, Y., Ao, C., Li, Y., Li, J., Li, H., Zhang, T., 2018. Late cretaceous–cenozoic thermochronology in the southern songliao basin, ne china: new insights from apatite and zircon fission track analysis. J. Asian Earth Sci. 160, 95–106.

Chlonova, A.F., 1961. Spores and pollen in the upper half of the Upper Cretaceous in the eastern part of the West Siberian lowland. Trudy Inst. Geol. Geofiz. Sibirsk. Otd. Akad. Nauk SSSR.

Cittert, K.V., 2002. Ecology of some Late Triassic to Early Cretaceous ferns in Eurasia. Rev. Palaeobot. Palyno. 119, 113–124.

Daqing Oilfield Petroleum Geography Compilation Group, 1993. China Petroleum Geology Vol. 2 Daqing and Jilin Oilfield (Volume 1). Petroleum Industry Press, Beijing (in Chinese).

Deng, C.L., He, H.Y., Pan, Y.X., Zhu, R.X., 2013. Chronology of the terrestrial Upper Cretaceous in the Songliao Basin, northeast Asia. Palaeogeogr. Palaeoclimatol. Palaeoecol. 385, 44–54.

Dettmann, M.E., 1973. Angiospermous pollen from Albian to Turonian sediments of eastern Australia. Geol. Soc. Aus. Spec. Pub. 4, 3–34.

Diessel, C.F.K., 1992. In: Coal-bearing Depositional Systems. Springer, pp. 721.

Doyle, J.A., 1969. Cretaceous angiosperm pollen of the Atlantic coastal plain and its evolutionary significance. J. Arnold Arboretum 50, 1–35.

Feng, Z., Jia, C., Xie, X., Zhang, S., Feng, Z., Cross, T.A., 2010a. Tectonostratigraphic units and stratigraphic sequences of the nonmarine Songliao basin, northeast China. Basin Res. 22, 79–95.

Feng, Z., Zhang, S., Cross, T.A., Feng, Z., Xie, X., Zhao, B., Fu, X., Wang, C., 2010b. Lacustrine turbidite channels and fans in the Mesozoic Songliao Basin, China. Basin Res. 22, 96–107.

Friedrich, O., Norris, R.D., Erbacher, J., 2012. Evolution of middle to Late Cretaceous oceans–A 55 m.y. record of Earth's temperature and carbon cycle. Geology 40, 107–110.

Gao, R., He, C., 1992. A New Genus and Species of Cretaceous Dinoflagellates from Two Transgressive Beds in Songliao Basin, NE China. Acta Palaeontol. Sin. 31, 17–29 (in Chinese with English abstract).

Gao, R., Zhao, C., Qiao, X., Zheng, Y., Yan, F., Wan, C., 1999. Cretaceous oil strata palynology from Songliao Basin. Geological Publishing House, Beijing (in Chinese).

Granger, H.C., Warren, C.G., 1969. Unstable sulfur compounds and the origin of roll type uranium deposits. Econ. Geol. 64, 160–171.

Heimhofer, U., Adatte, T., Hochuli, P.A., Burla, S., Weissert, H., 2008. Coastal sediments from the Algarve: low-latitude climate archive for the Aptian-Albian. Int. J. Earth Sci. 97, 785–797.

Hochuli, P.A., Menegatti, A.P., Weissert, H., Riva, A., Erba, E., Premoli Silva, I., 1999. Episodes of high productivity and cooling in the early Aptian Alpine Tethys. Geology 27, 657.

Hou, Q., Feng, Z., Feng, Z., 2009. Terrestrial petroleum geology of Songliao Basin. Petroleum Industry Press, Beijing (in Chinese).

Hu, X., 2004. Greenhouse climate and ocean during the Cretaceous. Geol. China 31, 442–448 (in Chinese with English abstract).

Huber, B.T., Norris, R.D., Macleod, K.G., 2002. Deep-sea paleotemperature record of extreme warmth during the Cretaceous. Geology 30, 123–126.

Ji, L., Zhang, M., Song, Z., 2015. The palynological record from Coniacian to lower Campanian continental sequences in the Songliao Basin, northeastern China and its implications for palaeoclimate. Cretac Res. 56, 226–236.

Jiao, Y., Wu, L., Peng, Y., Rong, H., Ji, D., Miao, A., Li, H., 2015. Sedimentary-tectonic setting of the deposition-type uranium deposits forming in the Paleo-Asian tectonic domain, North China. Earth Sci. Front. 22, 189–205 (in Chinese with English abstract).

Laing, J., 1975. Mid-Cretaceous angiosperm pollen from southern England and northern France. Palaeontology 18, 775–808.

Li, S., Xie, X., Wang, H., Jiao, Y., 2004. Sedimentary Basin Analysis: Principle and Application. Higher Education Press, Beijing (in Chinese).

Li, J., Zhang, Y., Cai, H., Guo, Z., Wan, X., 2008. Cretaceous and paleogene palynological successions at Zhongba, tibet and its significance. Acta Geol. Sin. 82, 584–593 (in Chinese with English abstract).

Li, J., Batten, D.J., Zhang, Y., 2011. Palynological record from a composite core through Late Cretaceous–early Paleocene deposits in the Songliao Basin, Northeast China and its biostratigraphic implications. Cretac Res. 32, 1–12.

Li, S.Q., Chen, F.K., Siebel, W., Wu, J.D., Zhu, X.Y., Shan, X.L., Sun, X.M., 2012. Late Mesozoic tectonic evolution of the Songliao basin, NE China: Evidence from detrital zircon ages and Sr-Nd isotopes. Gondwana Res. 22, 943–955.

Li, M., Zhao, Y., Liu, X., Zhang, Y., Wang, Y., 2009. Distribution of petroleum enriched areas, Changling Sag, Southern Songliao Basin. Petrol. Explor. Dev. 36, 413–418.

Liu, Z., Wang, D., Liu, L., Liu, W., Wang, P., Du, X., Yang, G., 1992. Sedimentary Characteristics of the Cretaceous in the Songliao Basin. Acta Geol. Sin. 66, 327–338 (in Chinese with English abstract).

Luo, Y., Ma, H.F., Xia, Y.L., Zhang, Z.G., 2007. Geologic characteristics and metallogenic model of Qianjiadian uranium deposit in Songliao basin. Uranium Geol. 23, 193–200 (in Chinese with English abstract).

Markevitch, V.S., 1994. Palynological zonation of the continental Cretaceous and lower Tertiary of eastern Russia. Cretac Res. 15, 165–177.

Mendes, M.M., Dinis, J.L., Gomez, B., Pais, J., 2010. Reassessment of the cheirolepidiaceous conifer Frenelopsis teixeirae Alvin et Pais from the Early Cretaceous (Hauterivian) of Portugal and palaeoenvironmental considerations. Rev. Palaeobot. Palyno. 161, 30–42.

Meng, Q.R., 2003. What drove late Mesozoic extension of the northern China-Mongolia tract? Tectonophysics 369, 155–174.

Min, M., Chen, J., Wang, J., Wei, G., Fayek, M., 2005a. Mineral paragenesis and textures associated with sandstone-hosted roll-front uranium deposits, NW China. Ore Geol. Rev. 26, 51–69.

Min, M., Xu, H., Chen, J., Fayek, M., 2005b. Evidence of uranium biomineralization in sandstone-hosted roll-front uranium deposits, Northwest China. Ore Geol. Rev. 26, 198–206.

Muller, J., 2010. Palynological evidence on early differentiation of angiosperms. Biol. Rev. 45, 417–450.

Nichols, D.J., Jacobson, S.R., 1982. Palynostratigraphic framework for the cretaceous (Albian-Maestrichtian) of the overthrust belt of Utah and Wyoming. Palynology 6, 119–147.

Nichols, D.J., Sweet, A.R., 1993. Biostratigraphy of Upper Cretaceous non-marine palynofloras in a north-south transect of the Western Interior Basin. Geol. Assoc. Can. Spec. Pap. 39, 539–584.

Nichols, D.J., Matsukawa, M., Ito, M., 2006. Palynology and age of some Cretaceous nonmarine deposits in Mongolia and China. Cretac Res. 27, 241–251.

Norris, G., Jarzen, D.M., Awai-Thorne, B.V., 1975. Evolution of the Cretaceous terrestrial palynoflora in western Canada. Geol. Assoc. Can. Spec. Pap. 13, 333–364.

Owen, D.E., Otton, J.K., 1995. Mountain wetlands: efficient uranium filters–potential impacts. Ecol. Eng. 5, 77–93.

Palynology Team, Institute of Botany, Academia, 1976. Sporae Pteridophytorum Sinicorum. Science Press, Beijing (in Chinese).

Pelzer, G., Riegel, W., Wilde, V., 1992. Depositional controls on the Lower Cretaceous Wealden coals of Northwest Germany. Geol. Soc. Am. 267, 227–244.

Rackley, R.I., 1972. Environment of Wyoming Tertiary uranium deposits. AAPG Bull. 56, 755–774.

Reynolds, R.L., Goldhaber, M.B., Carpenter, D.J., 1982. Biogenic and nonbiogenic ore-forming processes in the south Texas uranium district: evidence from the Panna Maria deposit. Econ. Geol. 77, 541–556.

Samoilovich, S.R., 1967. Tentative botanico-geographical subdivision of northern Asia in Late Cretaceous time. Rev. Palaeobot. Palyno. 2, 127–139.

Scott, R.W., Wan, X., Wang, C., Huang, Q., 2012. Late Cretaceous chronostratigraphy (Turonian-Maastrichtian): SK1 core Songliao Basin, China. Geosci. Front. 3, 357–367.

Skelton, P.W., Spicer, R.A., Kelley, S.P., Gilmour, I., 2003. The Cretaceous World. Cambridge University Press, Cambridge.

Song, Z., 1986. A review on the study of Early Cretaceous Angiosperm pollen in China. Acta Micropalaeontol. Sin. 3, 373–380 (in Chinese with English abstract).

Song, Y., Ren, J., Stepashko, A.A., Li, J., 2014. Post-rift geodynamics of the Songliao Basin, NE China: Origin and significance of T11 (Coniacian) unconformity. Tectonophysics 634, 1–18.
Stover, L.E., 1963. Some Middle Cretaceous Palynomorphs from West Africa. Micropaleontology 9, 85–94.
Sun, L.X., Zhang, Y., Zhang, T.F., Cheng, Y.H., Ma, H.L., Yang, C., Guo, J.C., Lu, C., Zhou, X.G., 2017. Jurrassic sporopollen of Yan'an Formation and Zhiluo Formation in the northeastern Ordos Basin, Inner Mongolia, and its paleoclimatic significance. Earth Sci. Front. 24 (1), 032–051 (in Chinese with English abstract).
Vakhrameyev, V.A., 1982. Classopollis pollen as an indicator of Jurassic and Cretaceous climate. Int. Geol. Rev. 24, 1190–1196.
Wan, X., Zhao, J., Scott, R.W., Wang, P., Feng, Z., Huang, Q., Xi, D., 2013. Late Cretaceous stratigraphy, Songliao Basin, NE China: SK1 cores. Palaeogeogr. Palaeoclimatol. Palaeoecol. 385, 31–43.
Wang, P., Chen, S., 2015. Cretaceous volcanic reservoirs and their exploration in the Songliao Basin, northeast China. Aapg Bull. 99, 499–523.
Wang, C., Feng, Z., Zhang, L., Huang, Y., Cao, K., Wang, P., Zhao, B., 2013a. Cretaceous paleogeography and paleoclimate and the setting of SKI borehole sites in Songliao Basin, northeast China. Palaeogeogr. Palaeoclimatol. Palaeoecol. 385, 17–30.
Wang, D., Liu, Z., Liu, L., 1994. Songliao Basin Evolution and Eustacy. Geological Publishing House, Beijing (in Chinese).
Wang, P., Liu, W., Wang, S., Song, W., 2002. 40 Ar/ 39 Ar and K/Ar dating on the volcanic rocks in the Songliao basin, NE China: constraints on stratigraphy and basin dynamics. Int. J. Earth Sci. 91, 331–340.
Wang, Y., Mosbrugger, V., Zhang, H., 2005b. Early to Middle Jurassic vegetation and climatic events in the Qaidam Basin, Northwest China. Palaeogeogr. Palaeoclimatol. Palaeoecol. 224, 200–216.
Wang, C., Scott, R.W., Wan, X., Graham, S.A., Huang, Y., Wang, P., Wu, H., Dean, W.E., Zhang, L., 2013b. Late Cretaceous climate changes recorded in Eastern Asian lacustrine deposits and North American Epieric sea strata. Earth Sci. Rev. 126, 275–299.
Wang, X., Wang, M., Zhang, X., 2005a. Palynology Assemblages and Paleoclimatic Character of the Late Eocene to Early Oligocene in China. Earth Sci. 30, 309–316 (in Chinese with English abstract).
Wu, B., 2005. Geology and Mineralization of Sandstone-Type Uranium Deposits in the Mesozoic-Cenozoic Basin in Northwest China. Northwest University, Xi'an (in Chinese with English abstract).
Wu, F.Y., Sun, D.Y., Ge, W.C., Zhang, Y.B., Grant, M.L., Wilde, S.A., Jahn, B.M., 2011. Geochronology of the Phanerozoic granitoids in northeastern China. J. Asian Earth Sci. 41 (1), 1–30.
Xia, Y., 2015. Qianjiadian Uranium Deposit. China Atomic Energy Press, Beijing (in Chinese).
Yang, Y., He, Z., 2016. Characteristics of Mesozoic-Cenozoic palaeoclimatic evolution and its constraint on mineralization of sandstone type uranium deposit in Junggar basin, Xinjiang, China. World Nucl. Geosci. 33, 140–145 (in Chinese with English abstract).
Yang, W.L., Li, Y.K., Gao, R.Q., 1982. Formation and evolution of nonmarine petroleum in the Songliao Basin, China. J. Chang. Inst. Geol. 1, 69–79 (in Chinese with English abstract).
Yoshino, K., Wan, X., Xi, D., Li, W., Matsuoka, A., 2017. Campanian-Maastrichtian palynomorph from the Sifangtai and Mingshui formations, Songliao Basin, Northeast China: Biostratigraphy and paleoflora. Palaeoworld 26, 352–368.
Yu, D., Wu, R., Chen, P., 2005. Geology of Uranium Resource. Harbin Engineering University Press, Heilongjiang (in Chinese).
Zhang, Y., 1981. Tertiary spores and pollen grains from the Leizhou Peninsula. Acta Palaeontol. Sin. 20, 69–122 (in Chinese with English abstract).
Zhang, Y., 1989. Late Cretaceous palynoflora from the western Tarim Basin of South Xinjiang, NW China. In: Cretaceous of the western Tethys. Proceedings of the International Cretaceous Symposium, Tubingen. Schweizerbartische Verlag, Stuttgart: E, pp. 779–788.
Zhang, Y., 1999. The evolutionary succession of Cretaceous angiosperm pollen in China. Acta Palaeontol. Sin. 38, 435–453 (in Chinese with English abstract).
Zhang, M., Dai, S., Heimhofer, U., Wu, M., Wang, Z., Pan, B., 2014. Palynological records from two cores in the Gongpoquan Basin, inner East Asia: evidence for floristic and climatic change during the Late Jurassic to Early Cretaceous. Rev. Palaeobot. Palyno. 204, 1–17.
Zhang, J.H., Gao, S., Ge, W.C., Wu, F.Y., Yang, J.H., Wilde, S.A., Li, M., 2010. Geochronology of the Mesozoic volcanic rocks in the Great Xing'an Range, northeastern China: implications for subduction-induced delamination. Chem. Geol. 276, 144–165.
Zhang, Y., Zhan, J., 1991. Late Cretaceous and Tertiary spores and pollen from the western Tarim Basin, Xinjiang, China. Science Press, Beijing (in Chinese).
Zhao, L., Cai, C.F., Jin, R.S., Li, J.G., Li, H.L., Wei, J.L., Guo, H., Zhang, B., 2018. Mineralogical and geochemical evidence for biogenic and petroleum-related uranium mineralization in Qianjiadian deposit, NE China. Ore Geol. Rev. 101, 273–292.
Zhao, J., Wan, X., Xi, D., Jing, X., Li, W., Huang, Q., Zhang, J., 2014. Late Cretaceous palynology and paleoclimate change: evidence from the SK1 (South) core, Songliao Basin, NE China. Sci. China: Earth Sci. 57, 2985–2997.
Zhao, B., Wang, C., Wang, X., Feng, Z., 2013. Late Cretaceous (Campanian) provenance change in the Songliao Basin, NE China: evidence from detrital zircon U-Pb ages from the Yaojia and Nenjiang Formations. Palaeogeogr. Palaeoclimatol. Palaeoecol. 385, 83–94.
Zhou, J.B., Wilde, S.A., Zhang, X.Z., Liu, F.L., Liu, J.H., 2012. Detrital zircons from phanerozoic rocks of the Songliao Block, NE China: evidence and tectonic implications. J. Asian Earth Sci. 47, 21–34.
Zhu, L., Tan, F., Fu, X., Chen, M., Feng, X., Zeng, S., 2012. Strata of the Late Mesozoic in the North of Qiangtang Basin: a discovery of the early cretaceous marine strata. Acta Sedimentol. Sin. 30, 825–833 (in Chinese with English abstract).
Zhu, G., Zhang, S., Katz, B.J., Su, J., Wang, X., Feng, Z., Cui, J., Liu, X., 2014. Geochemical features and origin of natural gas in heavy oil area of the Western Slope, Songliao Basin, China. Chem. Erde 74, 63–75.